https://doi.org/10.5194/cp-2023-85
Preprint. Discussion started: 7 November 2023

Climate of the Past Discussions

Hydroclimate extreme events detected by a sub-decadal diatom oxygen isotope record of the last 220 years from Lake Khamra, Siberia

Amelie Stieg[1], Boris K. Biskaborn[1], Ulrike Herzschuh[1,2,3], Jens Strauss[1], Luidmila Pestryakova[4], Hanno Meyer[1]

[1]Alfred Wegener Institute Helmholtz Centre for Polar and Marine Research, Potsdam, 14473, Germany.
[2]Institute of Geosciences, University of Potsdam, 14476, Germany.
[3]Institute of Biochemistry and Biology, University of Potsdam, 14476, Germany.
[4]Institute of Natural Sciences, North-Eastern Federal University of Yakutsk, Yakutsk, 677007, Russia.

Correspondence to: Amelie Stieg (amelie.stieg@awi.de)

https://doi.org/10.5194/cp-2023-85
Preprint. Discussion started: 7 November 2023

Climate of the Past Discussions
Open Access
EGU

Abstract. Northern latitudes have been significantly impacted by recent climate warming, which has increased the probability of experiencing extreme weather events. To comprehensively understand hydroclimate change and reconstruct extreme events such as droughts or floods, appropriate proxy records reaching further back in time are needed beyond meteorological measurements. Here we present a 220-year (2015-1790CE), gapless stable oxygen isotope record of diatoms ($\delta^{18}O_{diatom}$) from Lake Khamra (59.99° N, 112.98° E) in Eastern Siberia, an area highly sensitive to climate change and with a demand for palaeohydrological data. From a ^{210}Pb-^{137}Cs-dated sediment short core, this high-resolution proxy record was analysed to reconstruct hydroclimatic extremes on a sub-decadal scale. The interpretation of the $\delta^{18}O_{diatom}$ is supported by meteorological data, modern isotope hydrology, the ratio of planktonic-to-benthic diatom species and geochemical analyses of the same sediment indicative for the conditions in lake and catchment.

A comparison with meteorological data back to 1930 revealed that the $\delta^{18}O_{diatom}$ record of Lake Khamra is primarily influenced by regional precipitation changes rather than air temperature. We identified winter precipitation, which enters the lake as isotopically-depleted snowmelt water, as the key process impacting the diatom isotope variability. We related the overall depletion of $\delta^{18}O_{diatom}$ in recent decades to an observed increase in winter precipitation in the area, likely associated with the global air temperature rise, Arctic sea ice retreat and increased moisture transport inland. Available palaeoclimate proxy records, including a fire reconstruction of the same lake, support the new record as a valuable hydroclimate proxy indicative for precipitation deficits, tendentially excluding solar insolation and air temperature as driving forces even beyond meteorological recordings.

We identified two hydroclimatic extremes in the Lake Khamra $\delta^{18}O_{diatom}$ record, one at the beginning of the 19th century and a second prominent event in the 1950s. Both were interpreted as drought periods, associated with enriched $\delta^{18}O_{diatom}$ values likely caused by reduced winter precipitation and increased evaporation effects, which coincide with phases of reconstructed severe wildfires in the region. Despite the pristine lake area, we observed a triplication of mercury levels in the sediment record since the early 20th century, interpreted as an indication of human air pollution.

https://doi.org/10.5194/cp-2023-85
Preprint. Discussion started: 7 November 2023

Climate of the Past Discussions
Open Access
EGU

1 Introduction

Siberia has experienced an extraordinary heatwave during the initial six months of 2020 (Overland and Wang, 2020; Collow et al., 2022). This extreme event would have been highly improbable without human-induced climate change and even led to a new temperature record of 38°C, measured in the city Verkhoyansk, close to the Arctic Circle (Ciavarella et al., 2021). Recent climate change is faster in high northern latitudes as compared to the rest of the globe, a phenomenon known as Arctic Amplification (Manabe and Stouffer, 1980; Miller et al., 2010; Previdi et al., 2021). Since 1979, the northern latitudes have warmed nearly four times faster than the rest of the world (Rantanen et al., 2022) and this warming has even accelerated since the beginning of the 21st century (Chylek et al., 2022). Rapidly increasing air temperatures due to rising emissions of greenhouse gases caused by human activities result in higher frequency and/or intensity of extreme events (Seneviratne et al., 2021). Hydroclimate extreme events, including drought periods or intensified precipitation, are linked with ocean currents and large-scale dynamics. In the 21st century, Arctic precipitation is expected to increase drastically due to Arctic sea-ice retreat and increased evaporation (Bintanja and Selten, 2014; Bintanja, 2018).

The hydroclimate across Siberia has undergone notable alterations in recent decades, but differs regionally. While snow depth decreased over most southern parts of Russia, it increased in the northern parts including northern central Siberia (Ye et al., 1998). In addition, the snow cover duration was prolonged in Yakutia (Bulygina et al., 2009), the Republic of Sakha, located in the Russian Far East. In the past five decades, there has been a notable rise in overall precipitation levels across Yakutia (Gorokhov and Fedorov, 2018). Moreover, Yakutia is considered one of the most vulnerable regions for forest fires in ~~the country~~ (Kirillina et al., 2020). In 2021, Yakutia underwent its most severe fire season of the past forty years (Tomshin and Solovyev, 2022), highlighting an area of extremes. Meteorological records only start in the beginning of the 20th century, and there is a scarcity of high-resolution hydroclimate records predating this period. To reconstruct extreme hydroclimatic events and to analyse their occurrence and frequency, appropriate high-resolution proxy records are needed. Oxygen isotopes of lacustrine diatoms ($\delta^{18}O_{diatom}$) have been proven as valuable proxy to investigate temperature and hydrological variations in numerous studies (Leng and Barker, 2006; van Hardenbroek et al., 2018). $\delta^{18}O_{diatom}$ is influenced by different environmental and climatic factors, such as precipitation, evaporation or atmospheric circulation patterns, and is generally linked to variations in temperature and the oxygen isotope composition of the lake water ($\delta^{18}O_{lake}$; Leng and Barker, 2006; Meister et al., 2023). Nevertheless, influencing factors vary by location and have to be evaluated for each study site individually. Diatom oxygen isotope records located in Russia have been interpreted as palaeo-precipitation proxy (Chapligin et al., 2011; Kostrova et al., 2013a; Kostrova et al., 2013b; Meyer et al., 2022), to some extent sensitive to snow or glacier meltwater input (Kostrova et al., 2013b; Mackay et al., 2013; Kostrova et al., 2014; Meyer et al., 2015; Kostrova et al., 2021; Meyer et al., 2022) and dominated by summer temperatures on millennial timescales (Meyer et al., 2022). Furthermore, long-term trends in the $\delta^{18}O_{diatom}$ records correspond to those in summer insolation (Meyer et al., 2015; Kostrova et al., 2021; Meister et al., 2023) and teleconnections between Central Asia and the North Atlantic could be identified in one $\delta^{18}O_{diatom}$ record (Mackay et al., 2013). The available lake sediment $\delta^{18}O_{diatom}$ records predominantly cover the time period of the Holocene, and especially the last two thousand years (Meister et al., 2023). For Asia, there are 21 diatom isotope records published, with special emphasis on Siberia (Meister et al., 2023). However, the $\delta^{18}O_{diatom}$ records mainly focus on millennial time scales whereas high-resolution records of the past hundred years are very scarce. Moreover, we only found one Russian high-resolution study at Lake Baikal interpreted as a hydroclimate proxy (Swann et al., 2018).

https://doi.org/10.5194/cp-2023-85
Preprint. Discussion started: 7 November 2023

Climate of the Past Discussions
Open Access
EGU

This study aims to provide a new hydroclimate proxy record from Lake Khamra (59.99° N, 112.98° E) in Southern Yakutia. We hypothesise that a high-resolution $\delta^{18}O_{diatom}$ record can be used to reconstruct hydroclimate extreme events on a sub-decadal scale, such as drought events or prolonged rainfall periods since 1790. For this purpose, the latest 90 years of the record are validated by meteorological data to identify main drivers of the $\delta^{18}O_{diatom}$ record in the study area. Comparison with available palaeoclimate proxy records are used to assess key factors responsible for the diatom isotope variability and to analyse common trends beyond meteorological time scales. For the identification of large-scale dynamics, the $\delta^{18}O_{diatom}$ record is placed in the broader context of the northern landscape development. Additionally, we survey a possible human impact on this remote lake ecosystem since the onset of the industrial revolution.

https://doi.org/10.5194/cp-2023-85
Preprint. Discussion started: 7 November 2023

Climate of the Past Discussions
Open Access
EGU

2 Study area and regional climate

Figure 1. Study area. a) Position of Lake Khamra in the south-western part of Yakutia, close to the Lena river; closest weather station is located in Vitim, Lake Khamra lies in between the cities Yakutsk and Irkutsk. Comparable study sites are indicated as grey triangles (Jonsson et al., 2010; Swann et al., 2018; Broadman et al., 2022). b) Catchment of Lake Khamra, main in- and outflow are indicated by arrows. c) Sample locations at Lake Khamra. (Service layer credits: © OpenStreetMap contributors 2023. Distributed under the Open Data Commons Open Database License (ODbL) v1.0.; Esri, Maxar, Earthstar Geographics, and the GIS User Community).

https://doi.org/10.5194/cp-2023-85
Preprint. Discussion started: 7 November 2023

Climate of the Past Discussions
Open Access
EGU

Lake Khamra (59.99° N, 112.98° E, 340 m a.s.l.) is located in Eastern Siberia, in a sparsely populated area of south-west Yakutia (Republic of Sakha, Lensky District) in Russia. The closest urban settlements, Peleduy and Vitim, are situated 40 and 60 km south-west of the lake, respectively. The city of Yakutsk is located 930 km to the north-east, Irkutsk ca. 1000 km to the south-west (Fig. 1a).

Lake Khamra covers an area of 4.6 km² and has a catchment size of 107.3 km², extending towards the south-west. The water depth ranges from shallow shore areas towards a maximum of 22.3 m in the central part of the lake (Fig. 1c). There are several small tributaries flowing down the gentle hills into the lake, with the main inflow to the south-west and an outflow in the north-east (Fig. 1b). The lake is a hydrologically open system with an estimated average long-term discharge of 1.1 m³/s (0.03 km³/a) and an average residence time of the lake water of approximately 474 days (Messager et al., 2016). In winter, the lake is covered by ice and snow. During field work in March 2020, the ice thickness was on average half a metre and the snow cover was about one metre thick at different drilling locations (Biskaborn, 2021).

The lake is located within Cambrian bedrock comprising dolomite and limestone alternating with silty Ordovician sandstone and small delineated areas of clayey Silurian limestone (Chelnokova et al., 1988). The landscape is classified as mountain taiga within a discontinuous and sporadic permafrost zone (Brown et al., 1997; Fedorov et al., 2018). According to field observations, the catchment of the mountain lake Khamra is covered by a mixed-coniferous forest, mainly consisting of the tree species *Larix gmelinii*, *Picea obovata*, *Pinus siberica* and *Abies siberica* (Kruse et al., 2019; Miesner et al., 2022).

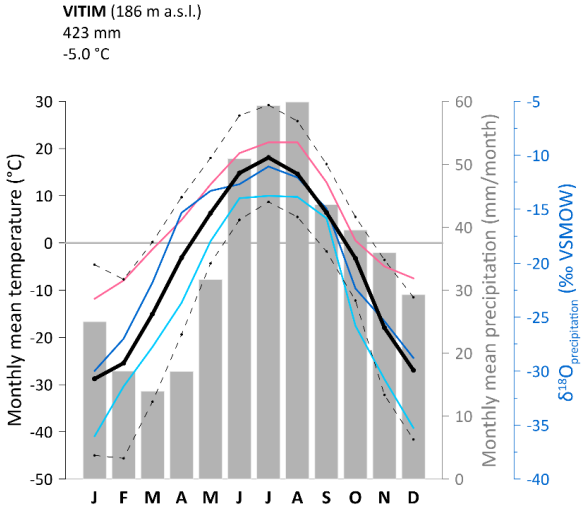

Figure 2. Meteorological data from the weather station Vitim (59.45° N, 112.58° E, 186 m a.s.l., ECA station code 3235), data accessible via the KNMI Climate Explorer https://climexp.knmi.nl: monthly mean precipitation amount 1929-2018, 90 yrs. (grey bars) and monthly mean temperature 1929-2018, 90 yrs. (black line; Klein Tank et al., 2002); daily max temperature 1930-2019 (upper dashed line) and min temperature 1928-2019 (lower dashed line, Durre et al. 2008). Monthly mean oxygen isotope values of precipitation ($\delta^{18}O_{prec}$) recorded in Yakutsk is shown by the light blue line (Kurita et al., 2004), recorded in Irkutsk is highlighted by the dark blue line (Kostrova et al., 2020). Modelled monthly $\delta^{18}O_{prec}$ values for the region (latitude 60°, longitude 113°, altitude 340 m) is shown as pink line (Bowen et al., 2005; Bowen, 2023; IAEA/WMO, 2023).

https://doi.org/10.5194/cp-2023-85
Preprint. Discussion started: 7 November 2023

Climate of the Past Discussions

According to the nearest weather station in Vitim (Fig. 1a) the region of Lake Khamra is strongly influenced by the continental climate (cf. Fig. 2), characterised by a large annual temperature range of 47°C from extremely cold and dry winters (lowest monthly mean in January: -28.8°C, 1929-2018) to warm and humid summer months (highest monthly mean July: +18.1°C, 1929-2018). The mean annual air temperature is -5.0°C with an annual mean precipitation amount of 423 mm (1929-2018), with most precipitation falling between June and September. All meteorological data were downloaded from the KNMI Climate Explorer website (https://climexp.knmi.nl), using data from the weather stations in Vitim (59.45° N, 112.58° E, 186 m a.s.l., ECA station code 3235, 1928-2019), Yakutsk (62.02° N, 129.72° E, 98 m a.s.l., ECA station code: 3214, 2019-1888) and Irkutsk (52.27° N, 104.35° E, 467 m a.s.l., ECA station code: 3245; 2018-1882; Klein Tank et al., 2002). For comparability with the weather station in Vitim, only meteorological data for the years 2018-1929 were considered.

The course of the oxygen isotope measurements of precipitation ($\delta^{18}O_{prec}$), recorded in Yakutsk (Kurita et al., 2004) and Irkutsk (Kostrova et al., 2020), follows the annual pattern of the temperature amplitude, with strongly depleted values in the winter months and more enriched values in summer (Yakutsk: January: -36.0‰, July: -13.8‰; Irkutsk: January: -30.0‰, July: -11.0‰; cf. Fig. 2). The modelled monthly $\delta^{18}O_{prec}$ values for the region (latitude 60°, longitude 113°, altitude 340 m) also fluctuate strongly over the course of the year (January: -23.3‰, July/August: -8.8‰; Bowen et al., 2005; Bowen, 2023; IAEA/WMO, 2023).

3 Methods

3.1 Water, ice, snow samples and stable isotope measurements

During two field campaigns, in August 2018 and in March 2020, samples were taken to analyse the isotopic composition of the lake water. During the summer field campaign in 2018, surface water (0-0.05 m) was sampled in the central part of the lake. Hydrophysical parameters like pH, conductivity and temperature of the lake water were specified.

In spring 2020, six water samples along a water depth profile were taken, below a lake ice cover of 0.65 m, which was additionally sampled. Two snow samples were collected near the shore within a profile of 60 cm (see map for the different sample locations, Fig. 1c).

The snow and ice samples were all completely melted and subsequently stored cool in 30 ml PE-bottles prior to stable isotope measurements. Hydrogen (δD) and oxygen ($\delta^{18}O$) isotopes were analysed at the ISOLAB Facility at the Alfred Wegener Institute Helmholtz Centre for Polar and Marine Research (AWI) in Potsdam, Germany, with mass spectrometers (DELTA-S Finnigan MAT, USA): hdl:10013/sensor.af148dea-fe65-4c87-9744-50dc4c81f7c9 and hdl:10013/sensor.62e86761-9fae-4f12-9c10-9b245028ea4c employing the equilibration method (details in Meyer et al. 2000). Data are given in per mil (‰) relative to Vienna Standard Mean Ocean Water (V-SMOW). N indicates the number of measurements per sample. If N>1, the mean isotope value of the sample was calculated from the individual measurement results. The standard deviation includes all measurements of the individual sample, which is generally better than the external (or machine) error. The external errors of long-term standard measurements for hydrogen and oxygen are better than ±0.8‰ and ±0.10‰, respectively (Meyer et al., 2000). The second order parameter deuterium excess (d excess) was computed according to: $d = \delta D - 8 * \delta^{18}O$ (Dansgaard, 1964).

https://doi.org/10.5194/cp-2023-85
Preprint. Discussion started: 7 November 2023

The water isotope samples of Lake Khamra are compared to the Global Meteoric Water Line (GMWL): $\delta D = 8 * \delta^{18}O + 10$ (Craig, 1961) and to Local Meteoric Water Lines (LMWL) based on the Global Network for Isotopes in Precipitation (GNIP) data (IAEA/WMO, 2023) recorded in Yakutsk (Kurita et al., 2004) and in Irkutsk (Kostrova et al., 2020). Additionally, for comparison the mean monthly and annual isotope composition of precipitation were modelled for the study area (latitude 60°, longitude 113°, altitude 340 m) using the Online Isotopes in Precipitation Calculator (OIPC; Bowen and Revenaugh, 2003; Bowen et al., 2005; Bowen, 2023; IAEA/WMO, 2023).

3.2 Sediment short core recovery and subsampling

During the field work in August 2018, a 42 cm sediment short core, EN18232-1, was retrieved from the central and deepest part of Lake Khamra (59.99091° N; 112.98373° E; water depth: 22.3 m) by using an UWITEC gravity corer (60 mm). The water depth was determined with a surveying rope and a handheld HONDEX PS-7 LCD digital sounder. After the field work, the sediment core was transported in a PVC tube to the AWI in Potsdam and stored dark and cool at 4°C until further analysis.

In October 2021, the short core was subsampled gapless in 1 cm increments (n=39). The rim material (<0.5 cm) of the individual sample layers was removed to avoid contamination by mixing sample material of different depths. With the help of a 1 cm^3 tool, additionally 24 subsamples were taken to determine the water content and dry bulk density (0-10 cm every 1 cm; >10 cm every 2 cm). All sediment samples were frozen and subsequently freeze dried for at least 48 h.

3.3 Dating

For establishing the high-resolution age-depth model, freeze-dried subsamples of the short core EN18232-1 (n=31) were analysed for ^{210}Pb, ^{226}Ra, ^{137}Cs and ^{241}Am by direct gamma assay in the Liverpool University Environmental Radioactivity Laboratory, using Ortec HPGe GWL series well-type coaxial low background intrinsic germanium detectors (Appleby et al., 1986).

With the intention of extending the ^{210}Pb-^{137}Cs age-depth model, subsamples (n=4) of the freeze-dried bulk material of the deeper part of the short core were sent to the radiocarbon analysis laboratory at AWI Bremerhaven. No plant macrofossils were found in the very fine-grained sample material and thus only bulk sediment samples were dated. ^{14}C was analysed by using an accelerator mass spectrometer (AMS) MICADAS (MIni CArbon Dating System; Mollenhauer et al., 2021) and calibrated with the IntCal20 ^{14}C calibration curve (Reimer et al., 2020), using the CALIB Radiocarbon Calibration Program (CALIB REV 8.2; Stuiver and Reimer, 1986, 1993).

To compute the age-depth model a Bayesian accumulation model within the R package 'rbacon' v2.5.8 (Blaauw and Christen (2011); R version 4.1.1) was used based on the ^{210}Pb chronology.

3.4 Diatom isotope purification process, $\delta^{18}O_{diatom}$ analysis and contamination correction

The diatom isotope purification process includes both chemical and physical preparation steps to obtain a purified diatom sample (Morley et al., 2004; Leng and Barker, 2006). 2 g aliquots of dried sediment samples (n=39) were processed for $\delta^{18}O_{diatom}$ analysis. The cleaning procedure is based on the processing steps described in Morley et

https://doi.org/10.5194/cp-2023-85
Preprint. Discussion started: 7 November 2023

Climate of the Past Discussions
Open Access
EGU

al. (2004) and refined in Kostrova et al. (2021). However, processing depends on the respective material and requires an individual approach (Leng and Sloane, 2008). The relevant steps applied are ~~mentioned~~ below. Organic matter was removed by adding H_2O_2 (30%, 50°C, ~55 h), followed by HCl (10%, 50°C, ~16 h) to eliminate carbonates. Before starting the heavy liquid separations (HLS), all samples were washed neutrally with ultra-pure water. By centrifuging the samples in sodium polytungstate solutions (SPT, $3Na_2WO_49WO_3*H_2O$) with decreasing densities (2.50-2.12 g/cm³), the diatoms were gradually separated from heavier impurities. An inverse HLS, described in detail in Kostrova et al. (2021), detached light micro-particles like charcoal from the diatom valves. To complete the purification process and remove possible residues of acid, SPT and clay minerals, all samples were washed neutrally with ultra-pure water using a 3 µm cellulose filter.

Contamination assessment of all processed samples (n=39), as well as of three heavy-liquid-separated samples (2.50 g/cm³), was carried out by a JEOL M-IT500HR analytical scanning electron microscope (SEM) with an integrated Energy-Dispersive X-ray Spectroscopy (EDS) system supplied with a Peltier element cooled SD detector (SDD) at AWI Potsdam. The standardless procedure was used according to Chapligin et al. (2012a) (six repetitions, acceleration voltage of 20.0 kV, magnification of 300, measuring time of 30 seconds). Detected elements are given as oxides with weight percentages. The focus is on the SiO_2 content as an indication of the purity of the processed sample and on Al_2O_3 as an indicator of contamination with clay fractions. The latter should be below 2.5% to avoid excessive shifts in the $\delta^{18}O_{diatom}$ record due to the correction (Chapligin et al., 2012a). EDS results, including the two oxides, are given in the appendices, Table A1. All 39 samples were highly purified and appropriate for $\delta^{18}O$ measurements, with an Al_2O_3 content ranging between 0.4 and 0.7% and with a SiO_2 content of 96.1 to 98.7%.

Before starting the isotope measurement, aliquots of the processed sample material were heated up at 1100°C by ramp degassing under a Helium flow to remove the exchangeable hydroxyl groups of the siliceous diatom cell walls applying the inert Gas Flow Dehydration method (iGFD; Chapligin et al., 2010). The oxygen isotope composition of the samples (n=39; additionally, heavy-liquid-separated minerogenic fraction, n=3) were measured at the ISOLAB Facility at AWI Potsdam with a semi-automated laserfluorination line (Chapligin et al., 2010) in combination with a SERCON HS2022 mass spectrometer. Thereby, the laser fluorination method was applied using bromine pentafluoride (BrF_5) as a reagent to completely release oxygen (Clayton and Mayeda, 1963) and convert the separated silicon to silicon tetrafluoride (SiF_4), which was transferred in glass tubes for further Si-isotope analysis (Leng et al., 2009) not included in this manuscript.

The oxygen isotopes were directly measured against international reference standards of known isotopic composition, given as delta notation ($\delta^{18}O$) relative to VSMOW in per mill (‰). Here we used the laboratory standards PS Jun17 ($\delta^{18}O$ = +43.61‰ ±0.16‰, n=13), calibrated against the marine standard PS1772-8 (Chapligin et al., 2010; Chapligin et al., 2011), and BFC 1 ($\delta^{18}O$ = +28.92‰ ±0.08‰, n= 19), calibrated against the standard biogenic silica (BFC; Chapligin et al., 2011). In addition, BDP-1 a new house internal control standard was introduced. Replicate analyses of BDP-1 yielded $\delta^{18}O$ = +26.89‰ ±0.25‰ (n=44) indicating an accuracy and analytical precision identical to the method's long-term analytical reproducibility (1σ) of ±0.25‰ (Chapligin et al., 2010). All samples were measured twice, partly three times. Analytical reproducibility of the sample material was ≤0.26‰.

All $\delta^{18}O$ measurements ($\delta^{18}O_{meas}$) were corrected ($\delta^{18}O_{corr}$) according to following geochemical mass-balance approach (Swann and Leng, 2009; Chapligin et al., 2012a):

$$\delta^{18}O_{corr} = (\delta^{18}O_{meas} - \frac{c_{HF*}\,\delta^{18}O_{HF}}{100})/(\frac{c_{diatom}}{100}) , \quad (1)$$

https://doi.org/10.5194/cp-2023-85
Preprint. Discussion started: 7 November 2023

Climate of the Past Discussions

To apply Eq. (1), the individual contamination percentages of each sample (c_{diatom}), the mean oxygen isotope value of the three heavy-liquid-separated samples ($\delta^{18}O_{HF}$ = +16.1 ±0.40‰, n=3) as well as their mean contamination percentages (c_{HF} = 11.3 ±0.39%, n=3) were used. The contamination percentage of each sample refers to the individual Al_2O_3 content of the EDS measurement results.

In order to increase comparability and to detect extreme events within the $\delta^{18}O_{diatom}$ record, the isotope values were standardised. Therefore, z-scores of each $\delta^{18}O_{diatom}$ value were calculated by subtracting the overall mean and dividing it by the standard deviation of the time series.

3.5 Further lake internal proxies

The inorganic carbon (TIC) content was determined of all 39 subsamples. Prior measurements, freeze-dried aliquots were milled to gain a homogeneous material. TIC was measured by using an Elementar soli TOC cube. The measurement accuracy was ±0.1%.

To detect possible heavy metal pollution within the sediment record, total mercury concentrations (THg) were quantified in all subsamples. THg was measured with a MLS-MWS DMA-80 evo III, given in µg/kg. The machine detection limit was 0.003 ng, with a laboratory proven limit of determination of 0.4 ng. All measurements were carried out at the Permafrost Carbon and Nitrogen Lab (CarLa) at AWI Potsdam.

Diatom slides were prepared for all 39 samples of the short core EN18232-1 to analyse the diatom species composition. The slide preparation followed the common procedure developed by Battarbee et al. (2001). Diatom valves were identified using the light microscope ZEISS AXIO Scope.A1 with a Plan-Apochromat 100x/ 1.4 Oil Ph3 objective at 1,000× magnification. A minimum of 350 diatom valves per sample were counted along transects. Diatom species were identified to lowest possible taxonomic level by using identification literature (Krammer and Lange-Bertalot, 1991; Krammer et al., 1991; Krammer and Lange-Bertalot, 1997b, a; Hofmann et al., 2011) and online databases (i.e., https://www.algaebase.org, https://www.diatoms.org). The ratio of planktonic-to-benthic diatoms (P/B ratio) was calculated, dividing the planktonic taxa by the sum of planktonic and benthic taxa (Wang et al., 2013). To calculate the ratio, habitat assignment follows the literature (Krammer and Lange-Bertalot, 1991; Krammer et al., 1991; Krammer and Lange-Bertalot, 1997b, a; Hofmann et al., 2011), online database (https://www.diatoms.org) and habitat information from Barinova et al. (2011). To compute the ratio, epiphytic taxa were included within the benthic species count. For some taxa, both planktonic and benthic habitats are possible (Barinova et al., 2011). If no exact assignment of species could be made with the help of further literature (Krammer and Lange-Bertalot, 1991; Krammer et al., 1991; Krammer and Lange-Bertalot, 1997b, a; Hofmann et al., 2011), the uncertain species were counted once as benthic (ratio 1) and once as planktonic (ratio 2) species.

https://doi.org/10.5194/cp-2023-85
Preprint. Discussion started: 7 November 2023

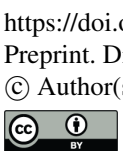

Climate of the Past Discussions
Open Access
EGU

4 Results

4.1 Water isotopes of Lake Khamra

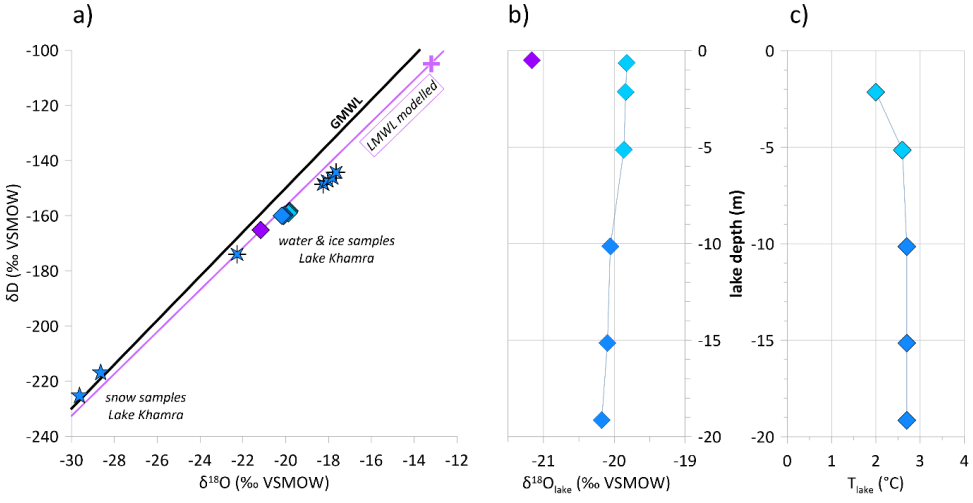

Figure 3. a) Co-Isotope plot ($\delta^{18}O$-δD) of lake water, ice and snow samples taken during the two field campaigns in 2018 (purple diamond) and 2020 (blue diamonds & stars), in relation to the GMWL (Craig, 1961). The LMWL according to the modelled monthly values is indicated as pink line. The modelled annual mean value is shown as cross (Bowen and Revenaugh, 2003; Bowen et al., 2005; Bowen, 2023; IAEA/WMO, 2023). b) $\delta^{18}O$ of water-depth profile of Lake Khamra, sampled below lake ice in March 2020 (blue diamonds). The purple diamond indicates the surface water sample taken in August 2018. c) T_{lake} of the water depth profile, taken below ice cover in March 2020.

Water, ice and snow isotope data sampled during the two field campaigns are shown in a $\delta^{18}O$-δD diagram (Fig. 3a). According to the surface water sample collected in summer 2018, $\delta^{18}O_{lake}$ has a value of -21.16‰, δD_{lake} of -165.3‰ and a d excess of +4.1‰ (n=1). The water sample has a pH of 6.07.

In March 2020, the total mean values of the water profile are isotopically heavier than the isotope values of 2018, whereby $\delta^{18}O_{lake}$ has a mean of -19.98‰ ±0.14‰, δD_{lake} of -159.3‰ ±0.7‰ and d excess of +0.5‰ ±0.5‰ (n=6). $\delta^{18}O_{lake}$ reveals only small variations of ±0.35‰ within the water profile and gets continuously lighter towards the bottom water (see Fig. 3b). The water temperature below the ice cover is quite low, varying from a minimum of 2°C to 2.7°C downwards (Fig. 3c). All measurements are listed in Table 1.

The ice cover of the lake, with a total thickness of 0.68 m, was sampled in 5 segments in March 2020 (see Table 1). The $\delta^{18}O$ values vary by ±4.62‰, with a minimum of -22.27‰ at the surface and a maximum of -17.65‰ at the transition from ice to water. δD ranges from -174.1‰ at the top to -144.3‰ at the bottom. This results in a positive d excess value of +4.0‰ in the upper ice sample and negative d excess values in the lower samples, down to -3.8‰.

The snow samples, collected close to the lakeshore, reveal the lowest $\delta^{18}O$ values with a mean of -29.14‰ and δD of -221.2‰, respectively, and a d excess of +11.9‰.

In comparison to the GMWL (Craig, 1961), only the two snow samples lie slightly above the GMWL, all water and ice samples of Lake Khamra lie slightly below the GMWL, and below or along the modelled LMWL of monthly values (Fig. 3a; Bowen et al., 2005; Bowen, 2023; IAEA/WMO, 2023). The modelled annual mean for

https://doi.org/10.5194/cp-2023-85
Preprint. Discussion started: 7 November 2023

Climate of the Past Discussions
Open Access
EGU

the region ($\delta^{18}O$: -13.2‰, δD: -105‰), is offset from the measurement results towards more enriched values (Fig. 3a; Bowen and Revenaugh, 2003; IAEA/WMO, 2023).

Table 1. Water, ice and snow samples from Lake Khamra, received in August 2018 and March 2020. The water temperature, measured in August 2018, is probably incorrect and not further used for interpretation. Conductivity of water sample EN18232 is given in µS/cm, conductivity of the water samples collected in March 2020 measured in mg/L.

Sample ID	Sample type	Sampling date	Sampling depth top (m)	Sampling depth bottom (m)	Lake Ice thickness (m)	δ18O H2O (‰ VSMOW)	1 std dv	δD H2O (‰ VSMOW)	1 std dv	d excess (‰)	N	Temperature (°C)	Conductivity (µS/cm, mg/L)
EN18232	water	2018-08-14	0.0	0.05	0	-21.16	0.03	-165.3	0.2	4.1	1	(21.7)	40
EN20001-01/0-5	water	2020-03-10	0.0	0.5	0.65	-19.82	0.02	-158.3	0.3	0.3	1		58
EN20001-01/1,5-2	water	2020-03-10	1.5	2.0	0.65	-19.84	0.01	-158.8	0.2	0.0	1	2.0	42
EN20001-01/4,5-5	water	2020-03-10	4.5	5.0	0.65	-19.87	0.03	-159.1	0.4	-0.2	1	2.6	45
EN20001-01/9,5-10	water	2020-03-10	9.5	10.0	0.65	-20.06	0.02	-159.8	0.4	0.7	1	2.7	50
EN20001-01/14,5-15	water	2020-03-10	14.5	15.0	0.65	-20.10	0.02	-160.1	0.4	0.6	1	2.7	53
EN20001-01/18,5-19	water	2020-03-10	18.5	19.0	0.65	-20.18	0.04	-160.0	0.3	1.4	1	2.7	61
EN20015/0-4/IceCore	ice core	2020-03-17	0.00	0.04	0.68	-22.27	0.10	-174.1	1.2	4.0	3		
EN20015/4-20/IceCore	ice core	2020-03-17	0.04	0.20	0.68	-18.25	0.15	-148.7	0.8	-2.7	3		
EN20015/20-36/IceCore	ice core	2020-03-17	0.20	0.36	0.68	-18.06	0.14	-147.4	0.4	-2.9	3		
EN20015/36-52/IceCore	ice core	2020-03-17	0.36	0.52	0.68	-17.83	0.21	-146.4	1.1	-3.8	2		
EN20015/52-68/IceCore	ice core	2020-03-17	0.52	0.68	0.68	-17.65	0.00	-144.3	0.0	-3.1	2		
EN20016/0-30/Snow	snow	2020-03-17	0.00	0.30		-28.64	0.11	-217.0	0.4	12.2	2		
EN20016/30-60/Snow	snow	2020-03-17	0.30	0.60		-29.63	0.16	-225.4	2.4	11.7	2		

4.2 Age-depth model

The sample material appeared very uniform in colour during sampling and no conspicuous stratifications were visible. The mean dry density of the short core EN18232-1 has a value of 114 ±38 mg/cm³, with a mean water content of 89 ±3% (n=24).

The homogeneity is also visible in the results of the ^{210}Pb and ^{137}Cs dating with a relative uniform accumulation at this site and a relatively uniform volumetric sedimentation rate of around 0.19 cm y^{-1}, with a slightly lower value since the 1950s (personal communication P. Appleby; visible in a slight flattening of the age-depth model in Fig. 4).

https://doi.org/10.5194/cp-2023-85
Preprint. Discussion started: 7 November 2023

Climate of the Past Discussions

According to the applied age-depth model based on the ^{210}Pb and ^{137}Cs dating, the short core, with a total length of 39 cm, spans a period of 222 years (2015-1793CE, mean ages). The mean sampling resolution of the record is sub-decadal with 5.7 ±1.7 years (min: 2, max: 10 years).

The four ^{14}C ages of the bulk sediment show a clear offset to the ^{210}Pb and ^{137}Cs chronology, with significant older ages (see Table 2). Comparing two dating results of the same sample depth (25-26 cm), we receive an ^{14}C age of 1806 ±20 ^{14}C years BP (before present) which corresponds to a calibrated ^{14}C age of 244 calibrated CE (2σ range: 210-256). The same sample was dated by the ^{210}Pb and ^{137}Cs method and received an age of 1858CE ±11. This results in a high offset of 1614 years. There are various explanations for this age offset (Björck and Wohlfarth, 2001). A comparable high age difference in the surface sample was observed in another study at Lake Khamra (Glückler et al., 2021), using macrofossil as well as bulk sediment samples to retrieve ^{14}C ages. Possible reasons were discussed such as an influence of dissolved carbonate rock, called hard-water effect (Björck and Wohlfarth, 2001; Philippsen, 2013), input of old organic carbon (Colman et al., 1996; Vyse et al., 2020) or mixing processes within the sediment (Biskaborn et al., 2012). Since the ^{210}Pb and ^{137}Cs dating results are very uniform reaching even a depth of 26 cm and no striking interruption could be detected during the sampling, a mixing process is rather unlikely. As shown in the other study from Lake Khamra (Glückler et al., 2021), very old macrofossils can be transported into the lake and possibly also influence the carbon age within the bulk sediment. The origin of the old carbon from eroding permafrost cannot be ruled out either, as the area lies in a sporadic permafrost zone (Brown et al., 1997; Fedorov et al., 2018). Additionally, inorganic carbon can be transported into the lake by the main inflow as the catchment contains early Palaeozoic carbonates (Chelnokova et al., 1988; Glückler et al., 2021). Large age uncertainties make it very difficult to use ^{14}C ages for records covering the last few hundred years (Björck and Wohlfarth, 2001). Since the old and non-continuous ^{14}C ages are not consistent with the homogeneous and high-resolution ^{210}Pb and ^{137}Cs dating results, the ^{14}C dating results are excluded from the age-depth model.

https://doi.org/10.5194/cp-2023-85
Preprint. Discussion started: 7 November 2023

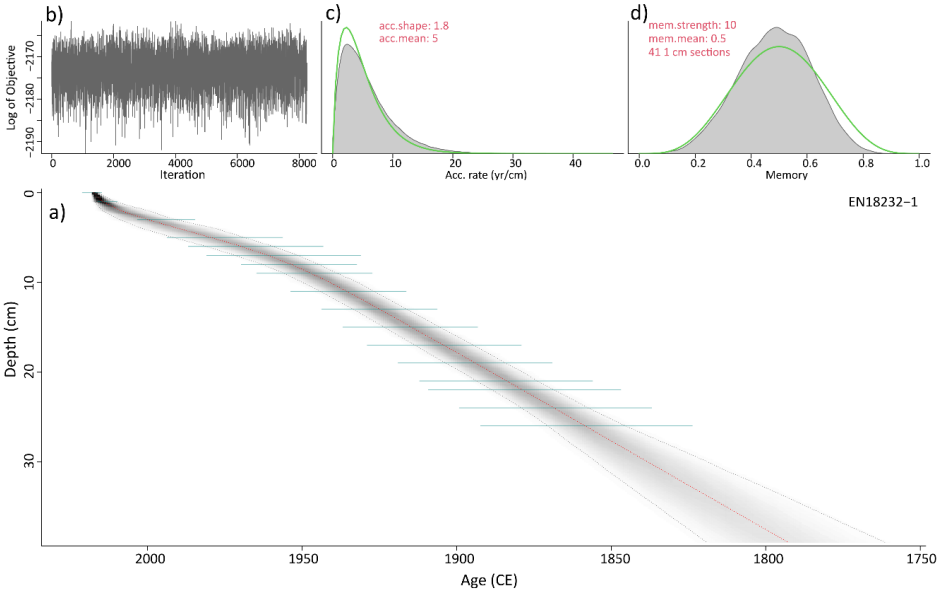

Figure 4. a) Bayesian accumulation model applying R package 'rbacon' (Blaauw and Christen, 2011) based on the ^{210}Pb and ^{137}Cs dating (green lines) of the short core EN18232-1 (grey lines=2σ range; red line=median). b) Model iteration log. c ,d) Prior (green line) and posterior (grey area) distributions for accumulation rate and memory, respectively.

Table 2. Results ^{14}C ages of the bulk sediment samples EN18232-1.

Lab-ID	Depth (cm)	F^{14}C	+- (abs)	^{14}C Age BP	+- (y)	Cal Age median [CE]	Cal Age min [CE] (2 sigma)	Cal Age max [CE] (2 sigma)	Cal Age median [BP]	Cal Age min [BP] (2 sigma)	Cal Age max [BP] (2 sigma)
EN18232-1_26	25-26	0.7987	0.0020	1,806	20	244	210	256	1706	1694	1740
EN18232-1_31	30-31	0.8415	0.0016	1,387	15	651	640	664	1299	1286	1310
EN18232-1_35	34-35	0.8708	0.0016	1,111	15	944	939	991	1006	959	1011
EN18232-1_38	37-38	0.8623	0.0016	1,190	15	842	818	888	1108	1062	1132

4.3 $\delta^{18}O_{diatom}$ record

The diatom δ^{18}O record of Lake Khamra (EN18232-1) covers approximately the last 220 years (2015-1790CE, mean ages; n=39). The overall mean $\delta^{18}O_{diatom}$ is +21.7‰ varying by ±2.8‰, with a standard deviation of ±0.6‰. The absolute minimum is +20.6‰ at 1941, 1915 and 1874. The absolute maximum of +23.4‰ occurs at 1953. Contamination correction increased all measured δ^{18}O values by a mean of +0.3‰ with a narrow range of between +0.2‰ and +0.4‰ (Fig. 5). This indicates a very low degree of contamination after cleaning, and an overall low correction within or close to the analytical error of ±0.25‰. The trend before and after contamination correction remains identical (-0.0006; n=39) which implies uniformly prepared sample material, where the correction has no

https://doi.org/10.5194/cp-2023-85
Preprint. Discussion started: 7 November 2023

Climate of the Past Discussions

(significant) effect on the course of the record. All descriptions refer to the corrected values (referred to as $\delta^{18}O_{diatom}$).

4.3.1 Phases of the Lake Khamra $\delta^{18}O_{diatom}$ record

We identify four phases (I-IV) into which the $\delta^{18}O_{diatom}$ time series of Lake Khamra is subdivided (Fig. 5). This differentiation from top to bottom of the core is mainly based on the deviation from the overall mean $\delta^{18}O_{diatom}$ value of +21.7‰. The description of phases begins with the most recent segment of the core and progresses towards the older sections, as the following discussion first validates the youngest part of the record with meteorological data.

Phase I (2015-1970, n=5)

In the most recent phase I, $\delta^{18}O_{diatom}$ of Lake Khamra shows values mostly below the overall mean with a low variability of ±1.2‰, a mean of +21.5‰ and a standard deviation of ±0.4‰. Main characteristics are a continuous decrease since 1970 with a clear minimum at 2000 (Fig. 5). Since 2000, $\delta^{18}O_{diatom}$ increases slightly, but still remains below the absolute mean value.

Phase II (1970-1930, n=6)

In contrast to phase I, $\delta^{18}O_{diatom}$ values in phase II are enriched in heavy isotopes above the overall mean including the absolute maximum (+23.4‰) at around 1950, with only one depleted value, a minimum, at about 1940 (+20.6‰). This results in the largest variability of ±2.8‰ of the entire $\delta^{18}O_{diatom}$ record , a clearly elevated mean value of +22.3‰ and a standard deviation of ±1‰. The maximum reaches a z-score of +2.7, the minimum has a negative score of -1.8.

Phase III (1930-1830, n=20)

Phase III consists of depleted $\delta^{18}O_{diatom}$ values, mainly below the overall mean, which begins rather abruptly around 1830 and persists until around 1930 whereby it varies by ±1.7‰. It is the longest phase of the diatom record (97 years), with the lowest mean value of all phases (+21.4‰), also including two absolute minima (+20.6‰ at 1915 and 1874), each with a z-score of -1.8. The standard deviation is comparable to phase I (±0.4‰).

Phase IV (1830-1790, n=8)

Phase IV of the Khamra record is characterised by notably enriched $\delta^{18}O_{diatom}$ values, primarily above the absolute mean. The internal mean of +22.2‰ is similar to phase II but less pronounced with a variability of ±1‰ and a standard deviation of only ±0.3‰ (Fig. 5).

https://doi.org/10.5194/cp-2023-85
Preprint. Discussion started: 7 November 2023

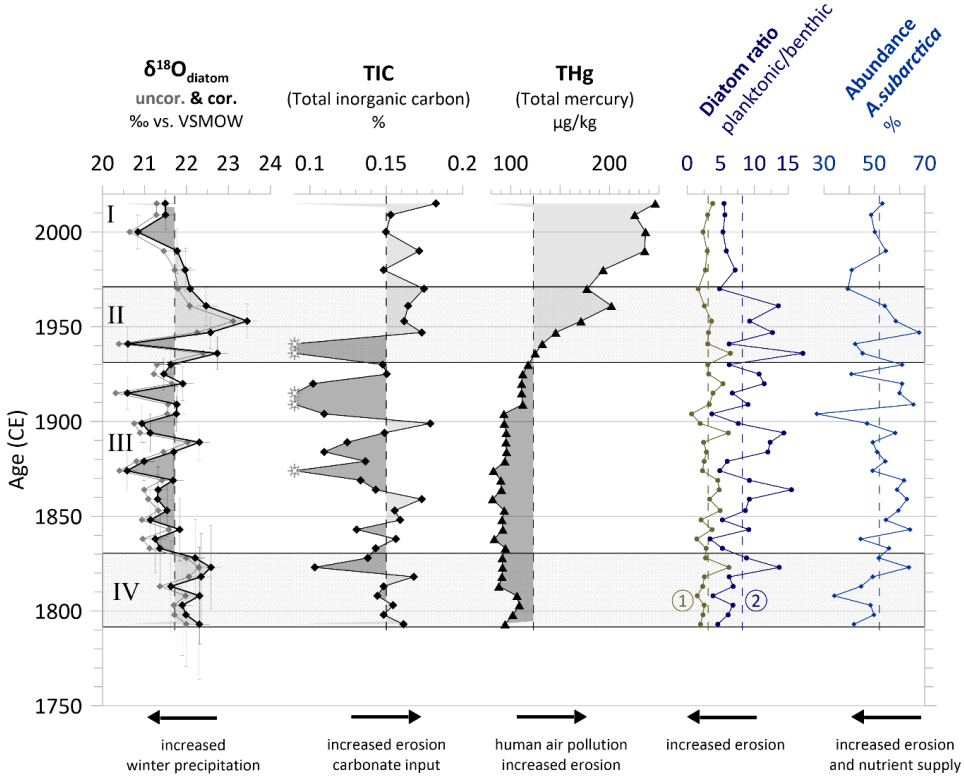

Figure 5. Lake internal proxy records of the short core EN18232-1, Lake Khamra. I-IV indicate the four phases according to the $\delta^{18}O_{diatom}$ record. Diatom $\delta^{18}O$: measured $\delta^{18}O_{diatom}$ (grey line) and contamination-corrected $\delta^{18}O_{diatom}$ values (black line) shown with analytical and chronological errors. Geochemical records: total inorganic carbon (TIC), white stars indicate values below detection limit. Total mercury (THg) given in µg/kg. Ratio of planktonic-to-benthic diatom species, ambiguous species counted to benthic (1), alternatively counted to planktonic habitat (2). Abundance of *Aulacoseira subarctica*, dominant diatom species of the short core, with an average occurrence of 52%. Vertical dashed lines indicate the individual mean values.

4.4 Carbon and mercury concentrations (TIC, THg) and diatom ratios

From the onset of the record at 1790 to the 1950s, TIC measurements remain constant at or slightly below the overall mean of 0.15%, interrupted by three maxima of 1.7% at 1820 and 1860, and 1.8% at 1900 (Fig. 5). At 1875, 1910 and 1940 five samples are below the detection limit of <0.1%. At 1950, TIC increases sharply and remains above the mean, towards another maximum of 1.8% in the uppermost sample.

THg shows a drastic increase and a tripling of the mercury levels in recent times (Fig. 5). All values are above the detection limit of 0.003ng. At the beginning of the record until around 1920, THg values fluctuate slightly between the minimum of 82 µg/kg to 111 µg/kg, but staying below the mean of 123 µg/kg. Since 1930, THg rises nearly continuously, reaching the maximum of 246 µg/kg in the topmost sample.

Diatoms occurred in all 39 samples. The planktonic species *Aulacoseira subarctica* (O. Müller) was the most represented diatom species (Fig. 5). At the beginning of the record until 1820, around 1900 as well as after the 1950s the abundance shows a clear reduction. The abundance is to some extent comparable to the planktonic-dominated P/B ratio (ratio 2, Fig. 5).

https://doi.org/10.5194/cp-2023-85
Preprint. Discussion started: 7 November 2023

Climate of the Past Discussions
Open Access
EGU

Both P/B ratios stay mainly below the mean until 1820 (mean values, ratio 1: 3.1 ; ratio 2: 8.2). Thereafter, the ratios fluctuate along the individual mean value. From 1960 onwards, the P/B ratios fall below the mean, with the change being more pronounced in the planktonic-dominated P/B ratio (ratio 2, Fig. 5).

https://doi.org/10.5194/cp-2023-85
Preprint. Discussion started: 7 November 2023

Climate of the Past Discussions

5 Discussion

5.1 Modern lake hydrology and isotopic signature of precipitation

The interpretation of the oxygen isotope record of lacustrine diatom silica ($\delta^{18}O_{diatom}$) requires a precise consideration of the current hydrological conditions of the respective study site (Leng and Barker, 2006). $\delta^{18}O_{diatom}$ is influenced directly and indirectly by various depleting and enriching factors, summarised in Meister et al. (2023). A direct fractionation process occurs during the temperature-dependent biosynthesis of the siliceous diatom shells, which enriches the $\delta^{18}O_{diatom}$ value compared to the lake water with a fractionation coefficient of -0.2‰/°C in lacustrine systems (Moschen et al., 2005; Dodd and Sharp, 2010). Beside the lake water temperature (T_{lake}), the oxygen isotope composition ($\delta^{18}O_{lake}$) and its sensitivity to evaporation ~~is~~ affecting the $\delta^{18}O_{diatom}$ signal. The water residence time of Lake Khamra has been modelled to about one year and three months (474 days; Messager et al., 2016), which implies a nearly annual exchange of the lake water and hence the possibility of only seasonal evaporative effects. The water depth-profile, taken below the spring ice cover, confirms a well-mixed water column with only slight variations of $\delta^{18}O_{lake}$ (±0.3‰) and no thermocline at least in March 2020 (Fig. 3b, c).

Lake Khamra is an open lake system, ~~due to its main inflow in the south-west and the~~ outflow in the north-east (see Map Fig. 1b). In open lake systems, $\delta^{18}O_{lake}$ generally mirrors the oxygen isotope signal of precipitation ($\delta^{18}O_{prec}$), including the local precipitation intermittency (Leng and Barker, 2006). We compare the lake isotope composition to the nearest stations of the Global Network of Isotopes in Precipitation (GNIP) in Yakutsk and Irkutsk (see map for different locations, Fig. 1a). The recent mean $\delta^{18}O_{lake}$ at Khamra lake of -20.0‰ (March 2020) is closest to the long-term annual weighted mean of Yakutsk (Fig. 6), but overall more depleted compared to annual weighted means both in Yakutsk ($\delta^{18}O_{prec}$: -19.2 ±1.8‰) and Irkutsk ($\delta^{18}O_{prec}$: -15.0 ±0.2‰; IAEA/WMO, 2023), respectively. The modelled annual mean $\delta^{18}O_{prec}$ of -13.2‰ is clearly shifted towards more enriched values compared to the lake water samples (Fig. 6). Consequently, the offset of $\delta^{18}O_{lake}$ towards depleted isotope composition indicates that the water of Lake Khamra is strongly influenced by isotopic light precipitation, likely snow or snowmelt originating during the cold winter months (see Fig. 2). The similarity of the $\delta^{18}O_{lake}$ measurements to the annual weighted mean $\delta^{18}O_{prec}$ of Yakutsk (Fig. 6) might be explained by the overall lowest monthly mean values of $\delta^{18}O_{prec}$ measured in Yakutsk, compared to Irkutsk and the regional modelled data (Fig. 2). $\delta^{18}O_{prec}$ is temperature-dependent and increases in the global mean at rising air temperatures (T_{air}) by +0.7‰/°C (Dansgaard, 1964). Ascribed to the more northerly position of Yakutsk (see map Fig. 1a), it reveals the coldest annual mean temperatures compared to Vitim and Irkutsk (-9.3°C, 1929-2018, Yakutsk, ECA station code: 3214) and thus most depleted $\delta^{18}O_{prec}$ (Dansgaard, 1964).

The Khamra $\delta^{18}O_{lake}$ measurements plot below the GMWL in the co-isotope plots (Figs. 3 and 6). The water samples measured in March 2020 plot even slightly below the LMWLs (Fig. 6), indicating potential evaporation effects at this site. The water samples taken in August and in March linearly correlate with a slope of 4.9 and an intercept of -60.6 (n=7, R^2=0.99), interpreted as evaporation line (EL; Fig. 6), comparable with local ELs of Central Yakutian lakes with a slope of 4.99 (n=39, R^2=0.95; Wetterich et al., 2008). The intersection point of the EL with the modelled LMWL ($\delta^{18}O$: -20.9‰, δD: of -164.0‰) is assumed to reflect the $\delta^{18}O$ of the mean influx to the lake and is nearly identical with the $\delta^{18}O_{lake}$ measurement of August 2018 ($\delta^{18}O_{lake}$: -21.2‰, δD_{lake} of -165.3‰). This suggests that the August-$\delta^{18}O_{lake}$-sample has a clear precipitation signal, not (or least) influenced by evaporation. The very low conductivity (40 µS/cm) of the surface lake water, measured in summer 2018, supports the assumption that for this sample evaporation effects are negligible.

https://doi.org/10.5194/cp-2023-85
Preprint. Discussion started: 7 November 2023

Climate of the Past Discussions

A strong depletion of this $\delta^{18}O_{lake}$ sample in comparison with the modelled regional annual mean of $\delta^{18}O_{prec}$ ($\delta^{18}O$: -13.20‰, δD: -105‰; Bowen and Revenaugh, 2003; Bowen, 2023; IAEA/WMO, 2023) is noticeable. In summer an isotopically heavier $\delta^{18}O_{lake}$ value would be expected due to higher summer temperatures, potential evaporation effects and the clear seasonality with enriched $\delta^{18}O_{prec}$ in the summer months (climate diagram: Fig. 2). However, the $\delta^{18}O_{lake}$ value measured in August 2018 is strongly depleted and corresponds to a modelled monthly mean value of precipitation between November and December (Fig. 2). Hence, the inflow of isotopically lighter water, for example through melt water from either snow and/or glaciers in the catchment, could lower $\delta^{18}O_{lake}$, as seen in other studies in Eurasia (Mackay et al., 2013; Meyer et al., 2015; Kostrova et al., 2021; Meyer et al., 2022). Lake Khamra lies at a relatively low altitude of 340 m a.s.l, without glaciers in the catchment that could be responsible for the depleted meltwater input. We know from an expedition report (Biskaborn, 2021), that a lot of snow can accumulate in this area as observed in March 2020. The snow samples taken from a 60 cm snow profile close to the lakeshore (Fig. 1c) during that expedition reveal the lowest isotope composition ($\delta^{18}O$ -29.1‰, δD of -221.2‰, d excess +11.9‰, n=2) of all analysed samples. Therefore, enhanced snow meltwater input could lead to an isotopic depletion of the lake water. Apparently, isotopically lighter waters can still be added to the water surface even in the summer months. However, since the difference of 1.2‰ to the water samples in March 2020 is not extreme and there is only one water sample measured in summer 2018, this single datapoint should be interpreted with caution.

Lake Khamra is an open lake system with a well-mixed water column and a quite uniform isotopic signature (as seen in March), influenced by precipitation with an important contribution of isotopically depleted water, likely snowmelt, leading to the overall low $\delta^{18}O_{lake}$. Moreover, evaporation likely has relatively small influence shifting the $\delta^{18}O_{lake}$ to only slightly enriched values below the LMWLs.

https://doi.org/10.5194/cp-2023-85
Preprint. Discussion started: 7 November 2023

Climate of the Past Discussions
Open Access
EGU

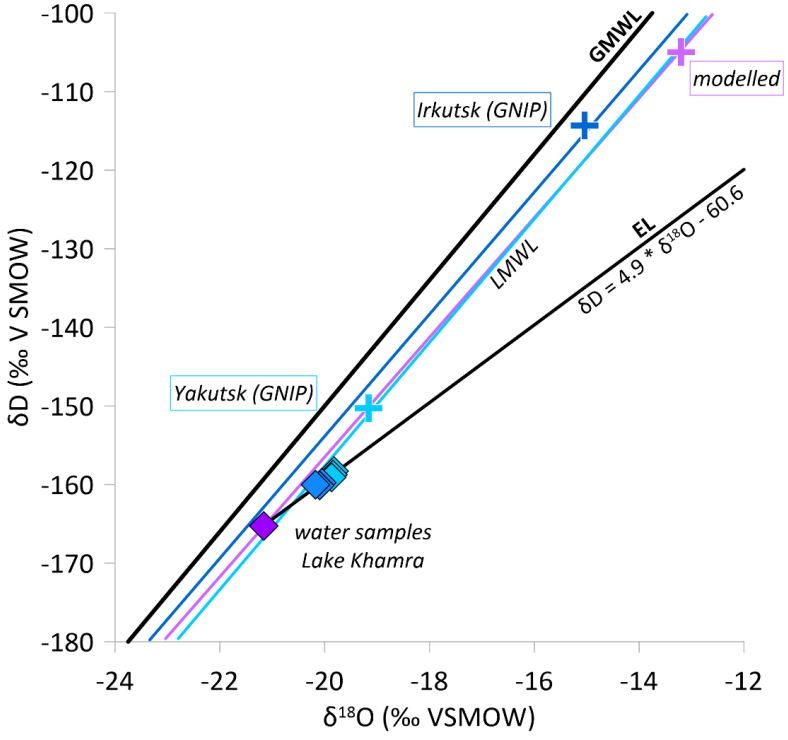

Figure 6. Co-isotope plot: Lake water samples of Lake Khamra (diamonds: purple=August 2018, blue=March 2020) compared to the Global Meteoric Water Line (GMWL; Craig, 1961) and Local Meteoric Water Lines (LMWLs) of Yakutsk (light blue line; Kurita et al., 2004), Irkutsk (blue line; Kostrova et al., 2020) and based on modelled monthly mean isotope values of precipitation (pink line) for the Khamra region (latitude 60°, longitude 113°, altitude 340 m; Bowen et al., 2005; Bowen, 2023; IAEA/WMO, 2023). Intercept point of the local evaporation line (EL) and modelled LMWL at $\delta^{18}O$: -20.9‰, δD: of -164.0‰. The weighted annual mean values of precipitation from the GNIP stations and the modelled annual mean are marked as crosses.

5.2 Drivers of $\delta^{18}O_{diatom}$

Different factors determine the isotopic signature of diatom shells (Leng and Barker, 2006; Meister et al., 2023), which is directly controlled by T_{lake} and $\delta^{18}O_{lake}$ during biosynthesis (Moschen et al., 2005; Dodd and Sharp, 2010). Leclerc and Labeyrie (1987) developed an equation based on the temperature-dependent fractionation between water and biogenic silica that can be used to reconstruct the water temperature conditions that prevailed during diatom shell formation.

Applying the following Eq. (2), we use the recent measured $\delta^{18}O_{diatom}$ = +21.5‰ and the mean $\delta^{18}O_{lake}$ = -20.0‰, measured in March 2020, to calculate a water-silica isotope fractionation factor of $\alpha_{(SiO2\text{-}H2O)}$ = 1.0423.

$$\alpha_{(SiO2-H2O)} = (1000 + \delta^{18}O_{diatom})/(1000 + \delta^{18}O_{lake}) \quad (2)$$

(Leclerc and Labeyrie, 1987)

Following the established isotope fractionation correlation, Eq. (3), between fossil diatom silica and water:

https://doi.org/10.5194/cp-2023-85
Preprint. Discussion started: 7 November 2023

Climate of the Past Discussions

$$1000 \ln \alpha_{(SiO2-H2O)} = 3.26 * 10^6/T^2 + 0.45 , \quad (3)$$

(Leclerc and Labeyrie, 1987)

we derive a T_{lake} of +8.7°C which is substantially higher than the mean T_{lake} = +2.45°C measured in March below the ice. If we calculate the T_{lake} with the isotope values measured in August 2018 ($\delta^{18}O_{lake}$ = -21.16‰; $\alpha_{(SiO2-H2O)}$ = 1.0436), we derive a temperature of +4.8°C. The calculated water temperature range (+4.8 to +8.7 °C) agrees very well with growth conditions of the diatom species *Aulacoseira subarctica (Gibson et al., 2003)*, almost predominant throughout the whole record of short core EN18232-1 (mean abundance: 52%, Fig. 5), and seems realistic in the early summer months when the ice cover of Lake Khamra starts to melt (May is the first month in which monthly mean T_{air}>0°C, 1928-2019, weather station Vitim).

It is assumed that in lake systems the effect of diatom species-dependent isotope fractionation, the so called vital-effect, is negligible (Shemesh and Peteet, 1998; Rosqvist et al., 1999; Shemesh et al., 2001; Leng and Barker, 2006; Chapligin et al., 2012b). *A. subarctica* is prevalent throughout the core and favours cold lake conditions at Lake Khamra. However, since there is only a very weak positive correlation between $\delta^{18}O_{diatom}$ and *A. subarctica* of +0.02 (p=0.05), a significant vital-effect on the $\delta^{18}O_{diatom}$ record can be excluded.

Using Eq. (3) with $\delta^{18}O_{lake}$ = -19.98‰ and T_{lake} = +2.45°C, measured in March 2020, we can also calculate an expected, recent $\delta^{18}O_{diatom}$ of +23.4‰. Hence, the calculated $\delta^{18}O_{diatom}$ is enriched by +1.9‰ compared to the actual measured surface $\delta^{18}O_{diatom}$ value (+21.5‰). This difference is likely due to the very low water temperature measured in March, which probably does not correspond to the diatom growth temperature as discussed above. Nevertheless, the reconstructed water temperatures seem realistic according to the dominant diatom species and the $\delta^{18}O_{diatom}$ record of Lake Khamra is generally assumed to be suitable for palaeoclimate reconstructions.

Globally T_{air} and $\delta^{18}O_{prec}$ have a positive fractionation coefficient of +0.7‰/°C (Dansgaard, 1964), which counterbalance the fractionation of biosynthesis between T_{lake} and $\delta^{18}O_{lake}$ (-0.2‰/°C, (Moschen et al., 2005; Dodd and Sharp, 2010). As a consequence, T_{air} has a stronger effect on $\delta^{18}O_{prec}$, linked with $\delta^{18}O_{lake}$ at Lake Khamra and therefore on $\delta^{18}O_{diatom}$. This tendency is visible in other $\delta^{18}O_{diatom}$ studies of the Northern Hemisphere (Meyer et al., 2015; Chapligin et al., 2016; Broadman et al., 2022). Using the dataset of the GNIP station in Yakutsk we can calculate a fractionation coefficient of +0.39‰/°C (n=12, monthly average values; 1969-2000, (IAEA/WMO, 2023) which is lower than the global coefficient but still clearly overprints the effect of T_{lake}. The coefficient is significantly higher (+0.81‰/°C) when we use the monthly average T_{air} values of the weather station in Vitim (60 km close to Lake Khamra; 1929-2018) and the monthly modelled $\delta^{18}O_{prec}$ values (n=12) for the region (Bowen et al., 2005; Bowen, 2023; IAEA/WMO, 2023). The distinct seasonality of $\delta^{18}O_{prec}$ highlights the strong T_{air} dependency at the Lake Khamra region, supported by the high annual T_{air} range of 47°C (Fig. 2). Therefore, we conclude the T_{air} dependent fractionation of precipitation overprints the fractionation due to biosynthesis and hence T_{air} has a stronger effect on the $\delta^{18}O_{diatom}$ record and its variations shape palaeoclimate trends rather than T_{lake}.

5.3 Comparison of $\delta^{18}O_{diatom}$ with meteorological data since 1930 including lake internal proxies

The comparison of the diatom record with meteorological data of Vitim, starting in the 1930s (Fig. 7), enables the validation of which factor best explains the variability of the $\delta^{18}O_{diatom}$ record, including T_{air}, evaporative effects, precipitation and seasonality, at least in the upper part of the record (phases I and II).

https://doi.org/10.5194/cp-2023-85
Preprint. Discussion started: 7 November 2023

Climate of the Past Discussions
Open Access
EGU

In phase I, we see an overall depletion of $\delta^{18}O_{diatom}$ values. Contrary, annual T_{air} rises and shows almost continuous positive anomalies since about the 1980s reaching up to +3.4°C at the weather station of Vitim (Fig. 7). Rising T_{air} would lead to enriched $\delta^{18}O_{prec}$ values (Dansgaard, 1964), followed by rising $\delta^{18}O_{lake}$ and $\delta^{18}O_{diatom}$ values. Moreover, an increase in T_{air} probably leads to stronger evaporative effects which would even further enrich $\delta^{18}O_{lake}$ and hence $\delta^{18}O_{diatom}$. If we assume T_{air} as major control, we would expect a continuous increase in $\delta^{18}O_{diatom}$. As a consequence, T_{air} cannot explain the observed, recent depletion in $\delta^{18}O_{diatom}$ and likely plays a subordinate role, at least in phase I.

However, during phase I, we see a significant increase in total rainfall amounts in the study area, illustrated by almost consistently positive annual precipitation anomalies (Fig. 7). An increase in precipitation in addition to rising temperatures would buffer evaporation effects and thus potentially weaken the increase of $\delta^{18}O_{lake}$ due to rising T_{air}. This is supported by the isotope composition of the recent lake water samples, which show only a minor effect of evaporation (Fig. 6).

In order to achieve a decrease in $\delta^{18}O_{diatom}$ resulting from higher precipitation levels, a greater quantity of isotopically light water has to reach the lake to be incorporated into the diatom frustules. Most depleted $\delta^{18}O_{prec}$ falls during cold seasons, mainly as snow, when regional mean monthly temperatures are below 0°C for 7 months (October to April; monthly mean T_{air} Vitim, see Fig. 2). We therefore disentangle the seasonal distribution of precipitation (Fig. 7). The majority of rainfall occurs during the summer months (June-July-August: JJA; Figs. 2 and 7). However, there is only a slight increase of the summer precipitation (JJA) observed in Vitim, while all three other seasons (September-October-November: SON; December-January-February: DJF; March-April-May: MAM) show more pronounced precipitation increases (Fig. 7). The highest increase is recorded during SON seasons (+0.61 mm/yr, R^2=0.2) and DJF (+0.60 mm/yr, R^2=0.5). Consequently, the overall increase in annual precipitation is likely mainly due to the increase in winter precipitation. Several studies discuss a change of snowfall amount over Eurasia in recent decades probably as a result of extreme temperature rises in the Arctic, leading to loss of sea ice and increased evaporation over the Arctic Ocean (Ghatak et al., 2010; Ghatak et al., 2012; Wegmann et al., 2015; Bailey et al., 2021; Sato et al., 2022). Increased moisture amounts are transported southwards leading to increased snowfall and duration of snow cover between 1966-2007 in specific areas in Eurasia, including Yakutia (Bulygina et al., 2009). Sato et al. (2022) confirms an increased moisture transport to Siberia in autumn and early winter months originating from the Arctic Ocean between 1981-2019 due to the retreat of sea ice, in line with observed expansion of snow cover.

During SON, the second largest amount of annual precipitation is received (Fig. 2), and thus it may contribute significantly to the isotopic signal of the lake water. During SON the mean temperatures fall rapidly below 0°C (monthly mean T_{air} Vitim: September: 6.4°C; October: -3.3°C; November: -18.0°C; 1929-2018). Consequently, most precipitation can be expected to fall as snow with highly depleted $\delta^{18}O$ values (see 4.1) which accumulates in the area and leads to a depletion of $\delta^{18}O_{lake}$ and, thus, of $\delta^{18}O_{diatom}$ when it reaches the lake as meltwater in the next spring season. This signifies an offset in seasonality in our diatom record, as the winter season and its snowfall do not affect the lake water and the diatoms therein before the following summer. Still, the sub-decadal resolution of our record needs to be considered, which precludes a record of annually resolved seasonal changes.

https://doi.org/10.5194/cp-2023-85
Preprint. Discussion started: 7 November 2023

Climate of the Past Discussions
Open Access
EGU

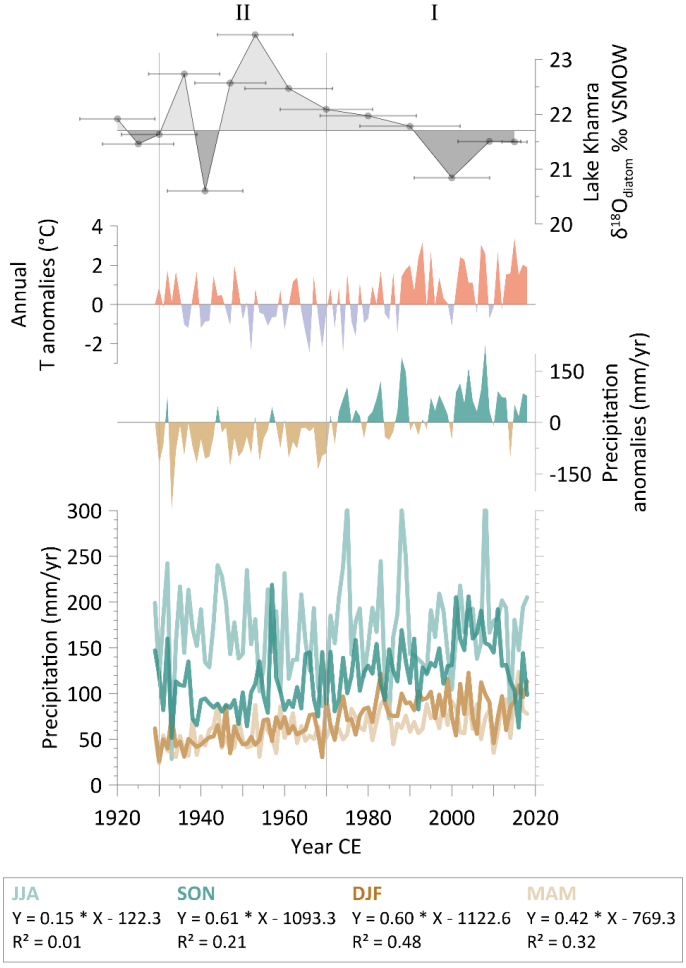

Figure 7. Khamra $\delta^{18}O_{diatom}$ record with age uncertainties of the corresponding phase I and II, compared to annual temperature anomalies and annual precipitation anomalies of Vitim, 1929-2018, 90 yrs., reference period 1961-1990. Below: Seasonal variation of precipitation amount 1929-2018, 90 yrs., displayed in different seasons: June, July, August (JJA), September, October, November (SON), December, January, February (DJF), March, April, May (MAM), individual trends are shown in the box. All meteorological data of weather station Vitim (59.45° N, 112.58° E, 186 m a.s.l.), ECA station code: 3235; data accessible via https://climexp.knmi.nl, (Klein Tank et al., 2002).

Nevertheless, periods of prolonged change in precipitation are likely to be reflected in the Khamra $\delta^{18}O_{diatom}$ record. From 2000 to 2010, significantly above-average precipitation amounts were measured in the SON as well as DJF and MAM season (assumed to mainly fall as snow with very low $\delta^{18}O_{prec}$). At this time, significantly depleted $\delta^{18}O_{diatom}$ values in the Khamra record (Fig. 7) indicate a significantly lower $\delta^{18}O_{lake}$, potentially caused by increased snowmelt input which directly influenced the main diatom bloom after ice break up. The influence of snowmelt and its varying amount as controlling factor of the diatom isotopy has been observed in other lacustrine $\delta^{18}O_{diatom}$ records in northern latitudes (Mackay et al., 2013; Rosqvist et al., 2013; Broadman et al., 2022; Meyer et al., 2022).

https://doi.org/10.5194/cp-2023-85
Preprint. Discussion started: 7 November 2023

Climate of the Past Discussions

Higher precipitation and increased snowmelt runoff are likely to increase erosion within Lake Khamra's catchment. Occurrence of dolomite and limestone in the bedrock of Lake Khamra (Chelnokova et al., 1988) is a possible source for elevated total inorganic carbon (TIC) values, probably contributing to the observed ^{14}C age offset (see 4.2). A study of the Russian lake Bolshoye Shchuchye uses TIC as a proxy for erosion (Lenz et al., 2021), supporting our argument for increased erosion by consistently above-average TIC values in phase I (Fig. 5). Mercury levels (THg) also exhibit a continuous increase and significant enrichment (Fig. 5), clearly surpassing the naturally occurring mercury concentrations measured in Yakutian permafrost, with a background signal of 5.21 ± 3.66 µg/kg (Rutkowski et al., 2021). Mercury is known to be deposited in lake sediments due to human pollution by different anthropogenic sources such as air fallout, erosion, mining, agriculture as well as industry and urban waste waters (Wang et al., 2004). Lake Khamra is very pristine, with no great industry or urban settlements in the close vicinity. It is likely that mercury reaches Lake Khamra by air pollution, comparable to Lake Bolshoe Toko, another pristine Russian lake (Biskaborn et al., 2021).

The abundance of the main diatom species *A. subarctica* shows a distinct reduction at the onset of phase I and recovers slightly, reaching up to 50% since the 1990s. *A. subarctica* favours low electrolyte level in the lake water (Krammer et al., 1991) and cold water temperatures (Gibson et al., 2003). Hence, rising temperatures in the area [illegible] increased erosion, increasing nutrient supply, could explain the reduction especially at the onset of phase I.

The diatom ratio of planktonic-to-benthic taxa (P/B ratio) can provide evidence for lake level fluctuations (Wolin and Stone, 2010). Increasing precipitation and probably negligible evaporation at Lake Khamra, as observed today, would be expected to raise the lake level and thus improve habitat conditions for planktonic species living in the water column. In contrast, both P/B ratios are below their mean values, showing both very low variability and a more benthic-dominated diatom assemblage in phase I. As for *A. subarctica*, rising temperatures and presumably higher erosion rates could have had a stronger, decreasing effect on planktonic diatom species than a general rise in lake level.

Contrary to conditions in phase I, phase II is metrologically characterised by a clear precipitation deficit, seen by negative annual anomalies, while temperatures indicate a rather moderate to cool period (Fig. 7). As in phase I and due to the positive correlation between T_{air} and $\delta^{18}O_{diatom}$, rather cool temperatures cannot explain the enriched $\delta^{18}O_{diatom}$ data, but the precipitation deficit may explain the elevated $\delta^{18}O_{diatom}$ values during phase II. From about 1935 to 1955, we see a clear deficit of SON precipitation (Fig. 7). If less snow has accumulated in autumn and winter, this leads to less meltwater input in the following spring and hence to less depleted $\delta^{18}O_{diatom}$ values. The influence of summer precipitation (JJA) on $\delta^{18}O_{lake}$ would even increase and, with its enriched $\delta^{18}O_{prec}$ values, could also lead to increased $\delta^{18}O_{diatom}$ values.

Both P/B ratios are above mean (Fig. 5), whereby the diatom ratio 2 shows a much higher variability, indicating more planktonic species as in phase I. In addition, the abundance of planktonic *A. subarctica* fluctuates strongly in phase II, reaches a maximum around 1950 and drops significantly towards the onset of phase I (Fig. 5). The dominance of planktonic species acts contrary to the observed precipitation deficit and a consequently expected lake level drop and less favourable habitat conditions for planktonic diatoms. Probably other factors, like insolation and temperature fluctuations, have positively influenced the growth conditions of planktonic diatoms and have a stronger influence on the diatom composition than the observed, nearly persistent precipitation deficit during phase II.

https://doi.org/10.5194/cp-2023-85
Preprint. Discussion started: 7 November 2023

Climate of the Past Discussions
Open Access
EGU

Between 1940 and 1950, TIC shows a striking shift from below detection limit to above mean values, comparable to variations seen in $\delta^{18}O_{diatom}$, the P/B diatom ratios and *A. subarctica* (Fig. 5). However, the sudden shift of TIC, and the assumed increase in erosion, cannot be explained by the observed precipitation deficit during that time and might be linked to an extreme event, discussed later on.

In addition, mercury levels start to rise rapidly since 1930 and show a first maximum around 1960, probably deposited by air pollution, as black carbon emissions quickly increased in Russia at that time (Eckhardt et al., 2023).

According to the correlation with meteorological data of Vitim, air temperature alone cannot be the driving factor of $\delta^{18}O_{diatom}$ at Lake Khamra. We assume that, at least in phase I and II, variability of precipitation is a key factor influencing the $\delta^{18}O_{diatom}$ signal. In particular, increased snowmelt water input, received during SON season, can explain the decreasing $\delta^{18}O_{diatom}$ trend in the recent decades. Contemporaneously, we identify an anthropogenic effect by drastically rising mercury levels in phase I and II.

5.4 Comparison of $\delta^{18}O_{diatom}$ and internal proxies beyond meteorological data

In contrast to phases I and II, there are no meteorological data for correlation covering phase III and IV. If we adopt the interpretation applied in phase I and II, the prolonged phase III, with the lowest $\delta^{18}O_{diatom}$ mean value of all four phases, suggests a phase of dominant winter precipitation, comparable to phase I and overall rather constant hydroclimatic conditions at Lake Khamra (Fig. 5).

Sufficient water supply into the lake would have increased or at least stabilised the lake water level and favoured the available habitat for planktonic species within the water column. The P/B ratios, which fluctuate around the mean, indicate overall rather good conditions for planktonic diatom species, comparable to the abundance of *A. subarctica* (Fig. 5). The high abundance of *A. subarctica* could, beside low salinity levels, also indicate cold water temperatures favoured by this diatom species (Gibson, 1981; Gibson et al., 2000; Gibson et al., 2003). Cool temperatures go along with generally more depleted $\delta^{18}O_{prec}$ values leading to reduced $\delta^{18}O_{diatom}$ values. Thus, together with possible increased winter precipitation, cold and wet periods have a reinforcing effect on $\delta^{18}O_{diatom}$, difficult to disentangle. Therefore, T_{air} as influencing factor cannot be ruled out completely in this part of the record and it is possible that the record will change from a precipitation-dominated to temperature-dominated regime, as seen in other studies (Meyer et al., 2015; Broadman et al., 2022; Meyer et al., 2022).

In line with favourable conditions for *A. subarctica*, TIC values vary mainly below the mean and show only short peaks towards increased values, indicating rather low erosional input from the catchment. However, TIC acts contrary to the interpretation in phase I, linking high erosion rates to increased snowmelt water supply. Mercury levels stay nearly consistent around 100 µg/kg, also seen in phase IV (Fig. 5), which can be assumed as the baseline value of the short core and does not yet show any influence of human air pollution during that time.

In phase IV, following the interpretation and comparable to phase II, we would expect a rather dry period with reduced winter precipitation linked with distinct enriched $\delta^{18}O_{diatom}$ values (Fig. 5). Both the P/B ratios as well as the abundance of *A. subarctica* switch from clearly below the mean to a maximum around 1820. Consequently, we would expect a lake level rise resulting in more favourable conditions for planktonic diatom species, unlike the $\delta^{18}O_{diatom}$ interpretation. TIC values start with slightly elevated values at the onset of the record and drop around

https://doi.org/10.5194/cp-2023-85
Preprint. Discussion started: 7 November 2023

Climate of the Past Discussions
Open Access
EGU

1820. Initially, a slightly increased erosion rate, seen by elevated TIC values, could lead to less favourable conditions for *A. subarctica*. However, higher temperatures, which also lead to enriched $\delta^{18}O_{diatom}$ values, might have resulted in less suitable conditions for *A. subarctica*. Similar to phase III, a warm and simultaneously dry phase could have amplified the diatom isotope signal.

In the older part of the record (phase III and IV) it stays yet indistinct, which factor is decisive for the $\delta^{18}O_{diatom}$ variability. Based on internal proxy interpretation, temperature cannot be ruled out as the prevailing influence on the diatom isotopy.

5.5 Comparison with regional to hemispherical proxy records

Prior to meteorological recordings, comparable high-resolution climate proxies of the region are rare. A charcoal record from a parallel sediment core of Lake Khamra (Glückler et al., 2021) is used as a regional wildfire proxy for the past 2200 years (Fig. 8). The "robust CHAR" record gives the charcoal accumulation rate over time (particles cm^{-2} yr^{-1}) by including chronology and counting uncertainties. Within the comparable time period the charcoal accumulation rate has two prominent maxima, one around 1950, the other at the early 1800s, both interpreted as increased fire activity in the area (Glückler et al., 2021). Both peaks in fire activity correspond very well with enriched $\delta^{18}O_{diatom}$ values observed in phases II and IV (Fig. 8). As persistent dry conditions favour forest fires, the overlap supports the interpretation of enriched $\delta^{18}O_{diatom}$ corresponding to dry conditions with reduced winter precipitation at Lake Khamra. A reduction in snow accumulation might lead to less soil moisture availability after snowmelt and, coinciding with higher temperatures, an early end of snowmelt can force extreme wildfires in eastern Siberia (Scholten et al., 2022). In contrast, periods of low fire activity, indicated by a low level of "robust CHAR" (Glückler et al., 2021), coincide with the assumption of rather wet periods with increased winter precipitation seen in phase I and III of the $\delta^{18}O_{diatom}$ record (Fig. 8). Snow accumulation might not only increase soil moisture but a prolonged snow cover duration, observed since 1966 in Yakutia (Bulygina et al., 2009), might also limit the duration of the subsequent annual fire season.

The maxima of the diatom record and in fire activity around 1950 coincide with the Modern Maximum of insolation (Coddington et al., 2015) and a temperature peak in the Northern Hemisphere (McKay and Kaufman, 2014). In contrast, the second charcoal maximum around 1800 overlaps with an insolation minimum (Dalton minimum) and the lowest temperature values of the comparable period (Fig. 8). Other diatom isotope studies on the Northern Hemisphere indicate a correlation with solar insolation, thus on millennial time scales (Swann et al., 2010; Kostrova et al., 2019; Kostrova et al., 2021; Meyer et al., 2022). Insolation of the sun mainly influences T_{air} and, thus, the isotopic signature of precipitation. The maximum in insolation coupled with higher temperatures do not contradict the interpretation of a dry period in phase II, whereby increased T_{air} could even amplify the enriched $\delta^{18}O_{diatom}$ values.

Nevertheless, the enriched $\delta^{18}O_{diatom}$ values in phase IV go along with reconstructed cold temperatures (McKay and Kaufman, 2014) and with the Dalton Minimum, a period of low sunspot activity between circa 1790 and 1830, which coincided with the eruption of Mount Tambora in Indonesia in 1815. This volcanic eruption is considered as one of the largest in recent centuries (Zielinski et al., 1994; Bradley, 2015) and had a global climate impact, resulting in significant drop of air temperatures and led, among others, to cooler ocean temperatures and an increase of the polar sea ice extent responding on decadal time scales (Stenchikov et al., 2009). In addition to the significant drop in air temperature, there was significantly less precipitation in many land regions, including regions north of

https://doi.org/10.5194/cp-2023-85
Preprint. Discussion started: 7 November 2023

Climate of the Past Discussions
Open Access
EGU

40° N, which had a lasting effect on the region for over a decade after the eruption (Kandlbauer et al., 2013). A moisture reconstruction from Northeast China for the period 1750 to 2015 based on tree ring $\delta^{18}O$, correlated with summer precipitation, relative humidity and drought intensity (Liu et al., 2022) also reports a dry period in the time period from 1750 to 1820.

The Dalton Minimum and the corresponding low temperatures must have had a subordinate effect on the $\delta^{18}O_{diatom}$ record, as the oxygen isotopes of diatoms are, in general, positively correlated with temperature and a reduction in temperature would lead to a depletion in diatom isotope values. As a consequence, increased $\delta^{18}O_{diatom}$ values in phase IV also likely correspond to dry conditions, and temperature as well as insolation can largely be excluded as driving force. Furthermore, the occurrence of dry conditions around these times serves as a potential explanation for high fire activity despite cool temperatures.

The cooler temperatures and the expanded sea ice coverage across the Arctic Ocean (Stenchikov et al., 2009) might have resulted in diminished inland moisture transport (especially during the winter months), potentially contributing to drier conditions in the Lake Khamra region during phase IV. The variability of snow accumulation, a main driver of $\delta^{18}O_{diatom}$ in this study, may depend on changing air-mass trajectories and changing moisture sources. In winter, between November and March, the Siberian high is predominant as a shallow high-pressure system above Central Siberia, due to strong radiational cooling over land associated with very cold and dry conditions (Shahgedanova, 2002). Winter precipitation is linked with frontal activity and mainly influenced by the Icelandic Low in the northwest and the Aleutian Low in the northeast linked to a depression in the upper troposphere (Mock et al., 1998; Shahgedanova, 2002). Thereby, moisture is generally transported from the Icelandic Low originating from the North Atlantic by westerly winds to Central Siberia (Shahgedanova, 2002). A 30-year smoothed and normalised Winter North Atlantic Oscillation (NAO) Reconstruction (Trouet et al., 2009) indicates high variability over the comparable time period (Fig. 8). Negative values signify a diminished pressure gradient and a weakening of the westerlies, resulting in a reduced eastward moisture transport potential (Hurrell, 1995; Osborn, 2006; Hurrell and Deser, 2010). This could favour dry conditions within the Khamra region, whereas a positive NAO phase can increase winter precipitation.

The significant negative NAO peak during phase II, accompanied by reduced winter precipitation and the transition to positive and thus possible snow-rich conditions corresponds to the meteorological data of the Khamra region and is consistent with the hydroclimatic interpretation of the diatom record.

A prevailing positive winter NAO phase between 1860 and the 1930s (Trouet et al., 2009), could have enhanced westerlies and promoted a moisture transport into the research area during winter. During that time, sufficient enhanced snowfall in winter and the later inflow as melt water could have contributed to a significant depletion of the lake water and hence of $\delta^{18}O_{diatom}$ in phase III (Fig. 8).

The strong negative phase in the NAO reconstruction between 1750 and 1800, does not directly correspond to the increased diatom values in phase IV. However, the diatom record begins around 1790 only and a previous significant negative NAO phase may have already favoured dry conditions in the region, promoted by the observed increase in fire frequency since 1750 (Glückler et al., 2021) and a dry period recorded by the moisture reconstruction from Northeast China (Liu et al., 2022).

Unfortunately, there is a scarcity of comparable high-resolution precipitation records within the study area. Nonetheless, we can exclude insolation as well as air temperature as main driving forces of the Khamra $\delta^{18}O_{diatom}$ record. The good agreement with the charcoal record and the winter NAO index contribute to identify past

https://doi.org/10.5194/cp-2023-85
Preprint. Discussion started: 7 November 2023

Climate of the Past Discussions

hydroclimate variability. This strengthens the assumption that variations in precipitation drive the $\delta^{18}O_{diatom}$ signal, extending to the earlier phases prior to meteorological observations.

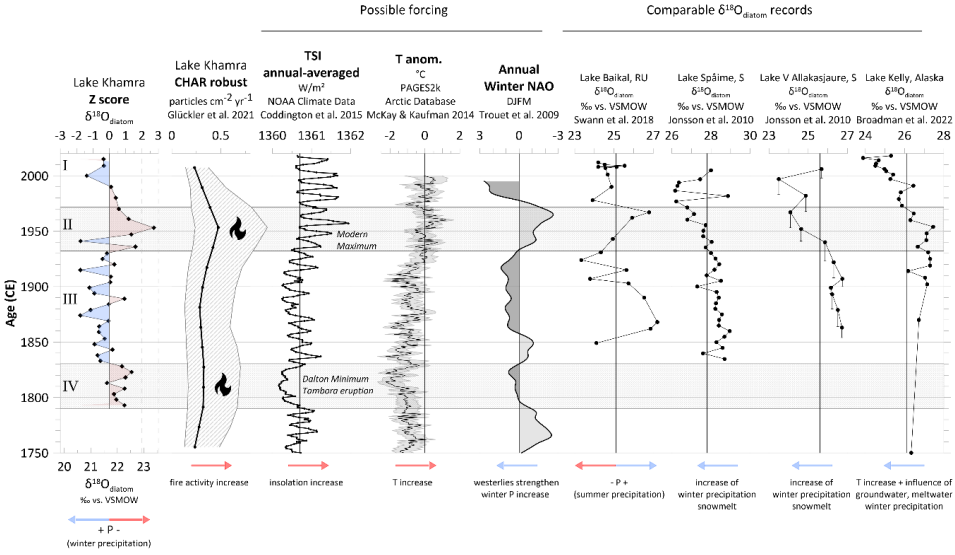

Figure 8. The Khamra diatom oxygen isotope record shown as absolute values and z-scores, in comparison to possible forcing and comparable diatom $\delta^{18}O$ records. The proxies for comparison include a charcoal record of Lake Khamra (Glückler et al., 2021), annual averaged total solar insolation TSI (Coddington et al., 2015), a reconstructed temperature anomaly for the Arctic (McKay and Kaufman, 2014) and a multi-decadal winter North Atlantic Oscillation (NAO) reconstruction (Trouet et al., 2009). Comparable $\delta^{18}O$ records include a record from Lake Baikal (Swann et al., 2018), two Swedish lakes (Jonsson et al., 2010), and a study from Alaska (Broadman et al., 2022). Arrows give individual interpretation. Vertical lines indicate the individual mean values.

5.6 Comparable high-resolution $\delta^{18}O_{diatom}$ records (regional and on the Northern Hemisphere)

There are very few high-resolution $\delta^{18}O_{diatom}$ records in northern latitudes covering the same time period that can be considered for comparison. For Russia we only found one high-resolution, decadal-scale diatom isotope study published by Swann et al. (2018). It includes a composite $\delta^{18}O_{diatom}$ record for the period 2010-1850 (160 yrs, n=21), originating from the southern basin of Lake Baikal, located circa 1000 km south of Lake Khamra (Fig. 1a). Swann et al. (2018) interpret the record as a hydroclimate proxy and conclude the Baikal $\delta^{18}O_{diatom}$ record mainly follows the river inflow composition, which reflects decadal changes of the Central Asian summer precipitation, strongly associated with the Atlantic Multidecadal Oscillation (AMO) in this region. The authors interpret their $\delta^{18}O_{diatom}$ values contrary to the Khamra record. Low values do not indicate an increase but a decrease in precipitation, presumably because the enriched isotope values of summer precipitation dominate the record linked with the Atlantic Multi-decadal Oscillation (Sun et al., 2015; Swann et al., 2018), rather than the heavily depleted winter precipitation as at Lake Khamra, which is linked with the NAO.

There are two high-resolution $\delta^{18}O_{diatom}$ records from high-altitude sub-Arctic lakes in Scandinavia (Figs. 1a and 8), covering the period from about 2005 to 1835 (Jonsson et al., 2010). Here, decreasing $\delta^{18}O_{diatom}$ values are linked with increased winter precipitation, entering the lake as snowmelt, coinciding with a high NAO index (Jonsson et al., 2010). This is a very similar interpretation to the Khamra lake record and supports the interpretation of diatom isotopes as proxy for winter precipitation and snowmelt. Similar context of snow-dominated lacustrine

https://doi.org/10.5194/cp-2023-85
Preprint. Discussion started: 7 November 2023


Climate of the Past Discussions

environments has been found for Kamchatka (Meyer et al., 2015) and the Polar Urals (Meyer et al., 2022), albeit on longer timescales.

In Alaska, a multi-proxy palaeoclimate study covering the Holocene encompasses two lakes on the Kenai Peninsula (Fig. 1a) and includes a high-resolution $\delta^{18}O_{diatom}$ record from Kelly Lake, spanning the last 120 years (1902-2018; Broadman et al., 2022). The record is interpreted as a hydroclimate proxy, where the temperature effect is also superimposed by various hydroclimatic variables (Leng and Barker, 2006; Broadman et al., 2022), corresponding to the $\delta^{18}O_{diatom}$ interpretation of Lake Khamra.

All $\delta^{18}O_{diatom}$ records of the three mentioned studies (Jonsson et al., 2010; Swann et al., 2018; Broadman et al., 2022) are significantly enriched in heavy isotopes compared to the Khamra $\delta^{18}O_{diatom}$ record (Fig. 8). The offset in $\delta^{18}O_{diatom}$ between these study sites is partly due to the northward position of Lake Khamra, coupled with considerably cooler T_{air}, or might be explained by the distinct continental climate of the Lake Khamra region and its reflection in $\delta^{18}O_{prec}$. All compared $\delta^{18}O_{diatom}$ records show a decreasing trend and a striking shift towards enriched $\delta^{18}O_{diatom}$ values in the youngest samples (Fig. 8). Lake Khamra record has no overall decreasing trend since 1850, but after 1950 the Khamra record shows a clear decreasing trend until 2000, with a rise in the youngest two samples (Fig. 8).

The Lake Baikal record (Swann et al., 2018) also has two minima at the onset of the 20th century and a maximum in the 1970s, comparable to the Lake Khamra record. The enriched $\delta^{18}O_{diatom}$ values between 1850 and 1950 do not fit to the observed overall below $\delta^{18}O_{diatom}$ mean values of the Khamra record in phase III. Extreme regional differences between these two lakes, such as catchment size and water residence time, as well as different development of summer and winter precipitation, probably lead to contrary interpretation.

Jonsson et al. (2010) reports a peak around 1980 in both Swedish $\delta^{18}O_{diatom}$ records (Fig. 8), delayed compared to the peak at the 1950s within the Khamra record, but also potentially attributed to a reduced ratio of winter to summer precipitation during that period. In general, the Swedish site shares similarities with the Khamra region in terms of NAO-driven winter precipitation fluctuations. Nevertheless, the $\delta^{18}O_{diatom}$ increase after 1990 is seen as a result of decreasing winter precipitation and simultaneous rising summer precipitation as well as rising annual temperatures (Jonsson et al., 2010), whereas winter precipitation and air temperature increased in the Lake Khamra region (Fig. 7). Remaining regional differences in hydroclimate, such as the influence of the Arctic Ocean on precipitation in the Khamra region, probably lead to the different extent of increase in the two records after 1990.

The $\delta^{18}O_{diatom}$ record of Kelly lake is similar to the Khamra record in phase I and II, with a maximum in the 1950s and a decrease afterwards. This decrease is related to an increasing amount of depleted winter precipitation due to a reduction of sea ice extent, depleted glacial meltwater originating from the glaciers, and/or depleted groundwater fed by glacial meltwater (Broadman et al., 2022). Unfortunately, there are no data available on groundwater conditions at Lake Khamra. Since there are no glaciers in the catchment of Lake Khamra, which could contribute to an isotopic decrease, the interpretation of Khamra $\delta^{18}O_{diatom}$ as winter precipitation proxy is strengthened.

The comparison with analogous high-resolution $\delta^{18}O_{diatom}$ records reveals similar hydroclimate reactions that support Lake Khamra's interpretation. The regional setting strongly influences the characteristics of each diatom record, requiring an individual consideration for data interpretation and cross-site comparisons. Nonetheless, this comparison strengthens the significance of the Khamra diatom record as a hydroclimate proxy, not only locally, but also cross-regionally with contrasting large-scale hydrological patterns.

https://doi.org/10.5194/cp-2023-85
Preprint. Discussion started: 7 November 2023

Climate of the Past Discussions
Open Access
EGU

5.7 Extreme events covered by Khamra $\delta^{18}O_{diatom}$ record

Investigations in this study reveal Khamra $\delta^{18}O_{diatom}$ record can be interpreted as a hydroclimate proxy focused on winter precipitation variability whereby T_{air} has a rather subordinate effect on $\delta^{18}O_{diatom}$. Hence, extreme values in the $\delta^{18}O_{diatom}$ record of Lake Khamra are most likely linked to dry (maxima) or wet (minima) phases. To identify extreme events in the Khamra diatom isotope record, we interpret phases of high variability and/or individual maxima.

An "extreme event", must be an event with a significant impact on precipitation changes, the lake water and its isotopic composition to see any effect in the $\delta^{18}O_{diatom}$ record. Considering that Lake Khamra's residence time is modelled to about one year and three months (474 days; Messager et al., 2016) and age uncertainties limit the resolution of our record, multi-day extreme events are unlikely to be captured by the diatom record. Consequently, the event in question must be of a "prolonged" or "persistent" nature (i.e. several dry or moist years in a row) to have an impact detectable within our sub-decadal diatom record.

The minima of the $\delta^{18}O_{diatom}$ record occur in phase III and in phase II, whereas the maximum occurs in phase II. Thus, the short phase II (1970-1930, n=6) is characterised by the highest variability, indicating the most extreme and rapidly changing environmental conditions within this record. The maximum in 1950 lies outside the 99% percentile and z-score analysis confirms the exceptionally high value, as it is the only one deviating by nearly 3 times the standard deviation within the record (Fig. 8). The maximum can be ruled out as a measurement error or outlier. On the one hand, the values before and after it support this maximum and, on the other hand, the sample has been measured in duplicate. Elevated $\delta^{18}O_{diatom}$ values correspond to elevated $\delta^{18}O_{lake}$ values, likely caused by diminished meltwater input, evident in a decrease in autumn (SON) precipitation between 1935 and 1950 and an overall period of precipitation deficit in the region until the late 1960s (Fig. 7). The precipitation reduction corresponds to a prolonged negative phase of winter NAO (Fig. 8), with a minimum in the 1960s (Trouet et al., 2009). Moreover, the striking maximum of the $\delta^{18}O_{diatom}$ record at 1950 coincides well with a clear maximum of the Khamra “robust CHAR” record (Glückler et al., 2021), indicating enhanced wildfire activity (Fig. 8). Vegetation surveys, carried out during the 2018 expedition (Kruse et al., 2019), revealed extensive regions of forest succession without less dense forest cover in the vicinity of Lake Khamra. Remote sensing data on historical forest fires and forest loss reach back to 2000 only (Hansen et al., 2013; Giglio et al., 2018). We suggest that wildfires, which occurred in the 1950s, had a considerable high impact destroying the dense forest in the lake’s vicinity and resulting in the formation of great forest succession areas afterwards, which can be even observed today. An observed increase of *Cyperaceae* pollen and more evergreen versus deciduous arboreal pollen types in the 1950s (Glückler et al., 2021), supports the assumption of a massive vegetation change in the vicinity of Lake Khamra after the 1950 fire event. Furthermore, *Cyperaceae* have the capability to promptly establish in recently disturbed and deforested regions, as after a wildfire, beside growing on wet areas (Glückler et al. 2021 and references therein: *Angelstam and Kuuluvainen, 2004; Isaev et al., 2010; Ivanova et al., 2014*).

The lake internal proxies also show a distinct shift at the time of $\delta^{18}O_{diatom}$ maximum. The TIC values suddenly rise from low, undetectable to significantly elevated values in the 1950s (Fig. 5). Assuming that a severe fire had suddenly led to an opening of previously dense forest vegetation in the catchment, the affected area, especially the soil cover, would likely become more vulnerable to erosion from rain and snowmelt flowing into the lake. Even years after the event, eroded soil material from the catchment is likely transported into the lake, in line with consistently elevated TIC values. Probably the first peak in THg around 1960 is related to these higher erosion rates (Fig. 5). In addition to anthropogenic mercury inputs by air from industrial activity, discussed in Sect. 5.3.,

https://doi.org/10.5194/cp-2023-85
Preprint. Discussion started: 7 November 2023

Climate of the Past Discussions
Open Access
EGU

mercury can not only be released into the air from burning plant material, but can also accumulate in burned soils where it can subsequently be transported to the lake by erosion (Burke et al., 2010).

Severe forest fires in the 1950s and the subsequent increased erosion has caused a change in water chemistry (TIC), potentially leading to increased salinity levels, less favourable for *A. subarctica* (Krammer et al., 1991). The second P/B diatom ratio also shows a clear shift from above to below mean values in the 1950s to the 1960s, indicating a reduction of planktonic species, such as *A. subarctica* (Fig. 5).

The same relationship between forest fires and increased $\delta^{18}O_{diatom}$ values can be seen around 1880, where a pronounced peak in the "classic" charcoal record, indicative of local fire occurrence, gives evidence for intense fires close to Lake Khamra (Glückler et al., 2021). TIC and mercury levels seem to react with elevated values shortly after the event (Fig. 5) and *A. subarctica* abundance drops to the lowest value of the whole record (Fig. 5). In addition, the elevated $\delta^{18}O_{diatom}$ values in phase IV overlap with the fire peak, slightly increased TIC and mercury values as well as a drop in *A. subarctica* (Fig. 5).

Extreme events in the form of prolonged dry periods, mainly due to a deficit of winter precipitation, form the basis for forest fires in this area. Extremes and hydroclimatic variability are reflected in the diatom isotope record of Lake Khamra, which agrees well with the reconstruction of forest fires in the lake. With age uncertainties and despite different temporal resolutions, reconstructed intense forest fires overlap with elevated $\delta^{18}O_{diatom}$ values.

https://doi.org/10.5194/cp-2023-85
Preprint. Discussion started: 7 November 2023

Climate of the Past Discussions
Open Access
EGU

6 Conclusions

The presented $\delta^{18}O_{diatom}$ record of Lake Khamra provides a valuable sub-decadal hydroclimate proxy record spanning from 1790 to 2015 for the understudied area of south-west Yakutia in Eastern Siberia. For the period of meteorological measurements since the 1930s, we could exclude air temperature as main driving factor of the variability of the $\delta^{18}O_{diatom}$ record of Lake Khamra. Instead, $\delta^{18}O_{diatom}$ is linked to seasonal precipitation changes in the region, especially to variations in early winter precipitation that enter the lake as isotopically depleted snowmelt water. An overall depletion of $\delta^{18}O_{diatom}$ since the 1950s is interpreted as an increase in winter precipitation in the area positively correlated with a winter NAO index. Prior to meteorological recordings, the $\delta^{18}O_{diatom}$ signal also appears to be little influenced by air temperature or solar insolation. The comparison with available palaeoclimate proxy records and other high-resolution $\delta^{18}O_{diatom}$ records of the Northern Hemisphere support the $\delta^{18}O_{diatom}$ record of Lake Khamra as a hydroclimate proxy, especially for winter precipitation shifts.

Hydroclimate extreme events are interpreted within the Lake Khamra $\delta^{18}O_{diatom}$ record as drought periods likely caused by reduced winter precipitation leading to enriched $\delta^{18}O_{diatom}$ values at the onset of the 19th century and especially in the 1950s. These two dry periods overlap with reconstructed wildfires in the area serving as a potential explanation for high fire activity despite overall rather cool temperatures. This shows that the reconstruction of hydroclimate extreme events is helpful to better understand climatic drivers of past fire activity.

Lake internal proxies, total inorganic carbon and mercury levels, support the interpretation of a dry period leading to severe wildfires in the 1950s by elevated values. TIC indicates an increase in erosion rates due to vegetation loss after possible severe fires by rising suddenly and permanently. The main planktonic diatom species *A. subarctica* appears to be sensitive to wildfire events, their possible effect on increased soil erosion and the subsequent, lasting changes in lake water chemistry. Synchronous with the peak of $\delta^{18}O_{diatom}$ around 1950, we detected a significant increase in mercury levels, which is only partially explainable by increased erosion after fire activity in the catchment and attributed to human air pollution, despite the remote location of Lake Khamra.

https://doi.org/10.5194/cp-2023-85
Preprint. Discussion started: 7 November 2023

Climate of the Past Discussions
Open Access
EGU

Appendices

Appendix A

Table A1. Main geochemical characteristics and isotopic signature of diatom samples from Lake Khamra. The purity of the sample material has been determined by EDS. SiO_2 content ranges between 96.1 and 98.7%, Al_2O_3 content between 0.4 and 0.7%. Mean $\delta^{18}O_{diatom}$ values (Diatom $\delta^{18}O_{mean}$), calculated contamination (%) and $\delta^{18}O$ values corrected for contamination (Diatom $\delta^{18}O_{corrected}$) are given.

Sample ID	Depth sed top (m)	Depth sed bottom (m)	Age (CE)	SiO2 (%)	Al2O3 (%)	Na2O (%)	MgO (%)	K2O (%)	CaO (%)	FeO (%)	total (%)	Diatom δ18O mean (‰ vs. SMOW)	Diatom δ18O std dev (±)	Repl (#)	Contamination (%)	Diatom δ18O corrected (‰ vs. SMOW)
EN18232-1-01	0.00	0.01	2015	96.59	0.44	2.55	0.11	0.12	0.08	0.19	100.08	21.29	0.17	2	3.85	21.50
EN18232-1-02	0.01	0.02	2009	96.75	0.46	2.40	0.07	0.12	0.06	0.15	100.01	21.29	0.26	3	4.03	21.50
EN18232-1-03	0.02	0.03	2000	97.42	0.46	1.73	0.06	0.07	0.07	0.20	100.00	20.65	0.17	2	4.06	20.84
EN18232-1-04	0.03	0.04	1990	96.54	0.64	2.33	0.04	0.16	0.04	0.25	100.01	21.46	0.20	2	5.65	21.78
EN18232-1-05	0.04	0.05	1980	97.07	0.49	2.04	0.06	0.10	0.07	0.19	100.01	21.72	0.24	3	4.31	21.97
EN18232-1-06	0.05	0.06	1970	96.05	0.55	2.97	0.11	0.14	0.06	0.17	100.04	21.80	0.21	2	4.84	22.09
EN18232-1-07	0.06	0.07	1961	96.47	0.69	2.43	0.06	0.09	0.07	0.21	100.02	22.08	0.06	2	6.14	22.47
EN18232-1-08	0.07	0.08	1953	97.13	0.52	1.98	0.05	0.12	0.06	0.16	100.01	23.11	0.22	2	4.59	23.45
EN18232-1-09	0.08	0.09	1947	96.45	0.55	2.58	0.08	0.13	0.07	0.19	100.04	22.26	0.09	2	4.85	22.57
EN18232-1-10	0.09	0.10	1941	98.60	0.54	0.44	0.06	0.05	0.11	0.21	100.00	20.39	0.14	2	4.77	20.60
EN18232-1-11	0.10	0.11	1936	96.70	0.57	2.25	0.07	0.15	0.07	0.19	100.00	22.40	0.11	2	5.08	22.73
EN18232-1-12	0.11	0.12	1930	97.72	0.69	1.09	0.08	0.11	0.08	0.24	100.00	21.30	0.26	2	6.08	21.63
EN18232-1-13	0.12	0.13	1925	98.66	0.50	0.46	0.04	0.04	0.10	0.22	100.00	21.22	0.10	2	4.38	21.46
EN18232-1-14	0.13	0.14	1920	97.07	0.51	2.05	0.03	0.11	0.06	0.18	100.00	21.66	0.13	2	4.47	21.92
EN18232-1-15	0.14	0.15	1915	97.90	0.70	0.94	0.06	0.11	0.08	0.21	100.00	20.32	0.21	2	6.16	20.59
EN18232-1-16	0.15	0.16	1909	97.45	0.43	1.77	0.05	0.08	0.08	0.17	100.02	21.56	0.16	2	3.76	21.78
EN18232-1-17	0.16	0.17	1904	96.57	0.44	2.65	0.07	0.09	0.07	0.14	100.03	21.54	0.05	2	3.85	21.76
EN18232-1-18	0.17	0.18	1899	97.37	0.43	1.77	0.06	0.06	0.09	0.25	100.04	20.76	0.21	2	3.82	20.94
EN18232-1-19	0.18	0.19	1894	98.40	0.56	0.71	0.04	0.04	0.09	0.18	100.01	20.89	0.02	2	4.91	21.13
EN18232-1-20	0.19	0.20	1889	96.25	0.50	2.92	0.07	0.10	0.07	0.15	100.05	22.03	0.14	2	4.43	22.31
EN18232-1-21	0.20	0.21	1884	97.24	0.49	2.00	0.06	0.03	0.06	0.15	100.01	21.45	0.24	2	4.29	21.69
EN18232-1-22	0.21	0.22	1879	97.16	0.42	2.15	0.05	0.06	0.07	0.13	100.03	20.81	0.05	2	3.69	20.99
EN18232-1-23	0.22	0.23	1874	98.53	0.46	0.74	0.04	0.02	0.08	0.15	100.03	20.40	0.26	3	4.09	20.59
EN18232-1-24	0.23	0.24	1869	97.31	0.53	1.85	0.05	0.04	0.07	0.17	100.02	21.42	0.15	2	4.71	21.68
EN18232-1-25	0.24	0.25	1864	97.63	0.71	1.19	0.09	0.10	0.09	0.19	99.99	20.99	0.06	2	6.32	21.32
EN18232-1-26	0.25	0.26	1859	97.82	0.49	1.42	0.07	0.02	0.07	0.14	100.02	21.09	0.16	2	4.29	21.31
EN18232-1-27	0.26	0.27	1853	97.86	0.44	1.45	0.04	0.02	0.04	0.17	100.01	21.33	0.22	2	3.87	21.54
EN18232-1-28	0.27	0.28	1848	98.37	0.46	0.84	0.04	0.02	0.09	0.19	100.01	20.94	0.10	2	4.07	21.14
EN18232-1-29	0.28	0.29	1843	97.25	0.50	1.93	0.04	0.03	0.10	0.19	100.02	21.58	0.15	2	4.46	21.84
EN18232-1-30	0.29	0.30	1838	97.91	0.66	1.06	0.06	0.09	0.04	0.18	100.00	20.96	0.15	2	5.84	21.26
EN18232-1-31	0.30	0.31	1833	97.55	0.54	1.54	0.06	0.05	0.10	0.18	100.01	21.12	0.22	2	4.74	21.37
EN18232-1-32	0.31	0.32	1828	97.31	0.39	1.96	0.07	0.03	0.08	0.18	100.01	22.00	0.05	2	3.44	22.21
EN18232-1-33	0.32	0.33	1823	97.19	0.51	2.01	0.05	0.03	0.07	0.17	100.02	22.29	0.01	2	4.49	22.58
EN18232-1-34	0.33	0.34	1818	97.62	0.52	1.53	0.03	0.04	0.09	0.19	100.02	22.06	0.01	2	4.60	22.34

https://doi.org/10.5194/cp-2023-85
Preprint. Discussion started: 7 November 2023

Climate of the Past Discussions

EN18232-1-35	0.34	0.35	1813	97.88	0.54	1.21	0.05	0.08	0.08	0.17	100.01	21.37	0.01	2	4.77	21.63
EN18232-1-36	0.35	0.36	1808	97.47	0.61	1.53	0.10	0.04	0.09	0.22	100.05	21.98	0.19	2	5.36	22.31
EN18232-1-37	0.36	0.37	1803	97.53	0.40	1.79	0.03	0.03	0.08	0.15	100.02	21.70	0.15	2	3.57	21.90
EN18232-1-38	0.37	0.38	1798	97.79	0.53	1.34	0.05	0.04	0.10	0.18	100.02	21.71	0.03	2	4.69	21.99
EN18232-1-39	0.38	0.39	1793	98.10	0.57	1.02	0.04	0.03	0.08	0.17	100.02	21.99	0.26	2	5.05	22.30

915

https://doi.org/10.5194/cp-2023-85
Preprint. Discussion started: 7 November 2023

Climate of the Past Discussions

Data availability

The datasets, including water isotope data, ^{14}C and ^{210}Pb-^{137}Cs dates, mercury, total inorganic carbon and the Khamra $\delta^{18}O_{diatom}$ record have been submitted to PANGAEA.

Authors contributions

AS, HM, BKB and UH designed the research project. BKB, UH and LP conducted fieldwork and received the sediment core and water samples in 2018 and 2020. AS processed and analysed the sediment samples in the lab, and together with HM interpreted the diatom and water isotope datasets. AS coordinated the sediment dating, did the age-depth modelling, performed diatom analysis and counting with the guidance of BKB. JS supervised mercury and inorganic carbon analysis and helped interpreting these proxies.

AS, HM and BKB structured the manuscript. AS produced all figures and tables and wrote the manuscript. All authors commented on drafts and have approved the final version.

Competing interests

The authors declare that they have no conflict of interest.

Disclaimer

Maps throughout this article were created using the Free and Open Source QGIS Geographic Information System. QGIS.org, Version 3.12, 2023 and the plugin 'Globe Builder' including OpenStreetMap data. This plugin is licenced with GNU Genereal Public License, version 2. This plugin uses OpenStreetMap Nominatim geocoding API, © OpenStreetMap contributors 2023. Distributed under the Open Data Commons Open Database License (ODbL) v1.0. .

Acknowledgments

We thank the teams of the ISOLAB Facility, the CarLa lab and the MICADAS radiocarbon laboratory of AWI. We would further like to thank Ramesh Glückler for his help sampling the sediment core and for his expertise in regional wildfire reconstruction, as well as all participants of the joint German-Russian expedition in Yakutia 2018 and 2020 for their support.

Funding details

Amelie Stieg is funded by AWI INSPIRES (International Science Program for Integrative Research in Earth Systems). The article processing charges for this open-access publication were covered by the Alfred Wegener Institute, Helmholtz Centre for Polar and Marine Research (AWI).

https://doi.org/10.5194/cp-2023-85
Preprint. Discussion started: 7 November 2023

Climate of the Past Discussions

7 References

Appleby, P. G., Nolan, P. J., Gifford, D. W., Godfrey, M. J., Oldfield, F., Anderson, N. J., and Battarbee, R. W.: 210Pb dating by low background gamma counting, Hydrobiologia, 143, 21-27, 10.1007/bf00026640, 1986.

Bailey, H., Hubbard, A., Klein, E. S., Mustonen, K.-R., Akers, P. D., Marttila, H., and Welker, J. M.: Arctic sea-ice loss fuels extreme European snowfall, Nature Geoscience, 14, 283-288, 10.1038/s41561-021-00719-y, 2021.

Barinova, S., Nevo, E., and Bragina, T.: Ecological assessment of wetland ecosystems of northern Kazakhstan on the basis of hydrochemistry and algal biodiversity, Acta Botanica Croatica, 70, 215-244, 10.2478/v10184-010-0020-7, 2011.

Battarbee, R. W., Jones, V. J., Flower, R. J., Cameron, N. G., Bennion, H., Carvalho, L., and Juggins, S.: Diatoms, in: Tracking Environmental Change Using Lake Sediments: Terrestrial, Algal, and Siliceous Indicators, edited by: Smol, J. P., Birks, H. J. B., Last, W. M., Bradley, R. S., and Alverson, K., Springer Netherlands, Dordrecht, 155-202, 10.1007/0-306-47668-1_8, 978-0-306-47668-6, 2001.

Bintanja, R.: The impact of Arctic warming on increased rainfall, Sci Rep, 8, 16001, 10.1038/s41598-018-34450-3, 2018.

Bintanja, R. and Selten, F. M.: Future increases in Arctic precipitation linked to local evaporation and sea-ice retreat, Nature, 509, 479-482, 10.1038/nature13259, 2014.

Biskaborn, B. K., Herzschuh, U., Bolshiyanov, D., Savelieva, L., and Diekmann, B.: Environmental variability in northeastern Siberia during the last ~ 13,300 yr inferred from lake diatoms and sediment–geochemical parameters, Palaeogeography, Palaeoclimatology, Palaeoecology, 329-330, 22-36, 10.1016/j.palaeo.2012.02.003, 2012.

Biskaborn, B. K., Narancic, B., Stoof-Leichsenring, K. R., Pestryakova, L. A., Appleby, P. G., Piliposian, G. T., and Diekmann, B.: Effects of climate change and industrialization on Lake Bolshoe Toko, eastern Siberia, Journal of Paleolimnology, 65, 335-352, 10.1007/s10933-021-00175-z, 2021.

Biskaborn, B. K., Bolshiyanov, Dmitry, Grigoriev, Mikhail N. , Morgenstern, Anne , Pestryakova, Luidmila A. , Tsibizov, Leonid and Dill, Antonia: Russian-German Cooperation: Expeditions to Siberia in 2020, 10.48433/BzPM_0756_2021, 2021.

Björck, S. and Wohlfarth, B.: 14C Chronostratigraphic Techniques in Paleolimnology, in: Tracking Environmental Change Using Lake Sediments: Basin Analysis, Coring, and Chronological Techniques, edited by: Last, W. M., and Smol, J. P., Springer Netherlands, Dordrecht, 205-245, 10.1007/0-306-47669-X_10, 978-0-306-47669-3, 2001.

Blaauw, M. and Christen, J. A.: Flexible paleoclimate age-depth models using an autoregressive gamma process, Bayesian Analysis, 6, 10.1214/11-ba618, 2011.

The Online Isotopes in Precipitation Calculator, version OIPC3.1: http://www.waterisotopes.org, last access: 18 October 2023.

Bowen, G. J. and Revenaugh, J.: Interpolating the isotopic composition of modern meteoric precipitation, Water Resour Res, 39, https://doi.org/10.1029/2003WR002086, 2003.

Bowen, G. J., Wassenaar, L. I., and Hobson, K. A.: Global application of stable hydrogen and oxygen isotopes to wildlife forensics, Oecologia, 143, 337-348, 10.1007/s00442-004-1813-y, 2005.

Bradley, R. S.: Paleoclimatology: Reconstructing Climates of the Quaternary, 3rd ed, Academic Press, San Diego [u.a.] 9780123869135, 2015.

Broadman, E., Kaufman, D. S., Anderson, R. S., Bogle, S., Ford, M., Fortin, D., Henderson, A. C. G., Lacey, J. H., Leng, M. J., McKay, N. P., and Muñoz, S. E.: Reconstructing postglacial hydrologic and environmental change in the eastern Kenai Peninsula lowlands using proxy data and mass balance modeling, Quaternary Research, 107, 1-26, https://doi.org/10.1017/qua.2021.75, 2022.

Brown, J., Ferrians Jr, O. J., Heginbottom, J. A., and Melnikov, E. S.: Circum-Arctic map of permafrost and ground-ice conditions, Report 45, 10.3133/cp45, 1997.

Bulygina, O. N., Razuvaev, V. N., and Korshunova, N. N.: Changes in snow cover over Northern Eurasia in the last few decades, Environmental Research Letters, 4, 10.1088/1748-9326/4/4/045026, 2009.

Burke, M. P., Hogue, T. S., Ferreira, M., Mendez, C. B., Navarro, B., Lopez, S., and Jay, J. A.: The Effect of Wildfire on Soil Mercury Concentrations in Southern California Watersheds, Water Air Soil Pollut, 212, 369-385, 10.1007/s11270-010-0351-y, 2010.

https://doi.org/10.5194/cp-2023-85
Preprint. Discussion started: 7 November 2023

Chapligin, B., Narancic, B., Meyer, H., and Pienitz, R.: Paleo-environmental gateways in the eastern Canadian arctic - Recent isotope hydrology and diatom oxygen isotopes from Nettilling Lake, Baffin Island, Canada, Quaternary Science Reviews, 147, 379-390, 10.1016/j.quascirev.2016.03.028, 2016.

Chapligin, B., Meyer, H., Bryan, A., Snyder, J., and Kemnitz, H.: Assessment of purification and contamination correction methods for analysing the oxygen isotope composition from biogenic silica, Chemical Geology, 300-301, 185-199, 10.1016/j.chemgeo.2012.01.004, 2012a.

Chapligin, B., Meyer, H., Swann, G. E. A., Meyer-Jacob, C., and Hubberten, H. W.: A 250 ka oxygen isotope record from diatoms at Lake El'gygytgyn, far east Russian Arctic, Clim Past, 8, 1621-1636, 10.5194/cp-8-1621-2012, 2012b.

Chapligin, B., Meyer, H., Friedrichsen, H., Marent, A., Sohns, E., and Hubberten, H. W.: A high-performance, safer and semi-automated approach for the delta18O analysis of diatom silica and new methods for removing exchangeable oxygen, Rapid Commun Mass Spectrom, 24, 2655-2664, 10.1002/rcm.4689, 2010.

Chapligin, B., Leng, M. J., Webb, E., Alexandre, A., Dodd, J. P., Ijiri, A., Lücke, A., Shemesh, A., Abelmann, A., Herzschuh, U., Longstaffe, F. J., Meyer, H., Moschen, R., Okazaki, Y., Rees, N. H., Sharp, Z. D., Sloane, H. J., Sonzogni, C., Swann, G. E. A., Sylvestre, F., Tyler, J. J., and Yam, R.: Inter-laboratory comparison of oxygen isotope compositions from biogenic silica, Geochim Cosmochim Ac, 75, 7242-7256, 10.1016/j.gca.2011.08.011, 2011.

Geologic map of Yakutia P-48,49, 1 : 1000000, VSEGEI, Leningrad: http://www.geokniga.org/sites/geokniga/, last access: 11.11.2022.

Chylek, P., Folland, C., Klett, J. D., Wang, M., Hengartner, N., Lesins, G., and Dubey, M. K.: Annual Mean Arctic Amplification 1970–2020: Observed and Simulated by CMIP6 Climate Models, Geophysical Research Letters, 49, 10.1029/2022gl099371, 2022.

Ciavarella, A., Cotterill, D., Stott, P., Kew, S., Philip, S., van Oldenborgh, G. J., Skalevag, A., Lorenz, P., Robin, Y., Otto, F., Hauser, M., Seneviratne, S. I., Lehner, F., and Zolina, O.: Prolonged Siberian heat of 2020 almost impossible without human influence, Clim Change, 166, 9, 10.1007/s10584-021-03052-w, 2021.

Clayton, R. N. and Mayeda, T. K.: The use of bromine pentafluoride in the extraction of oxygen from oxides and silicates for isotopic analysis, Geochim Cosmochim Ac, 27, 43-52, 10.1016/0016-7037(63)90071-1, 1963.

Coddington, O., Lean, J. L., Lindholm, D., Pilewskie, P., Snow, M., and Program, N. C.: NOAA Climate Data Record (CDR) of Total Solar Irradiance (TSI), NRLTSI Version 2 [dataset], 10.7289/V55B00C1 2015.

Collow, A. B. M., Thomas, N. P., Bosilovich, M. G., Lim, Y.-K., Schubert, S. D., and Koster, R. D.: Seasonal Variability in the Mechanisms behind the 2020 Siberian Heatwaves, Journal of Climate, 35, 3075-3090, 10.1175/jcli-d-21-0432.1, 2022.

Colman, S. M., Jones, G. A., Rubin, M., King, J. W., Peck, J. A., and Orem, W. H.: AMS radiocarbon analyses from Lake Baikal, Siberia: Challanges of dating sediments from a large, oligotrophic lake, Quaternary Science Reviews, 15, 669-684, 10.1016/0277-3791(96)00027-3, 1996.

Craig, H.: Isotopic Variations in Meteoric Waters, Science, 133, 1702-1703, 10.1126/science.133.3465.1702, 1961.

Dansgaard, W.: Stable isotopes in precipitation, Tellus A: Dynamic Meteorology and Oceanography, 16, 10.3402/tellusa.v16i4.8993, 1964.

Dodd, J. P. and Sharp, Z. D.: A laser fluorination method for oxygen isotope analysis of biogenic silica and a new oxygen isotope calibration of modern diatoms in freshwater environments, Geochim Cosmochim Ac, 74, 1381-1390, https://doi.org/10.1016/j.gca.2009.11.023, 2010.

Durre, I., Menne, M. J., and Vose, R. S.: Strategies for evaluating quality assurance procedures, Journal of Applied Meteorology and Climatology, 47, 1785-1791, 10.1175/2007jamc1706.1, 2008.

Eckhardt, S., Pisso, I., Evangeliou, N., Zwaaftink, C. G., Plach, A., McConnell, J. R., Sigl, M., Ruppel, M., Zdanowicz, C., Lim, S., Chellman, N., Opel, T., Meyer, H., Steffensen, J. P., Schwikowski, M., and Stohl, A.: Revised historical Northern Hemisphere black carbon emissions based on inverse modeling of ice core records, Nat Commun, 14, 271, 10.1038/s41467-022-35660-0, 2023.

Fedorov, A., Vasilyev, N., Torgovkin, Y., Shestakova, A., Varlamov, S., Zheleznyak, M., Shepelev, V., Konstantinov, P., Kalinicheva, S., Basharin, N., Makarov, V., Ugarov, I., Efremov, P., Argunov, R., Egorova, L., Samsonova, V., Shepelev, A., Vasiliev, A., Ivanova, R., Galanin, A., Lytkin, V., Kuzmin, G., and Kunitsky, V.: Permafrost-Landscape Map of the Republic of Sakha (Yakutia) on a Scale 1:1,500,000, Geosciences, 8, 10.3390/geosciences8120465, 2018.

https://doi.org/10.5194/cp-2023-85
Preprint. Discussion started: 7 November 2023

Ghatak, D., Frei, A., Gong, G., Stroeve, J., and Robinson, D.: On the emergence of an Arctic amplification signal in terrestrial Arctic snow extent, Journal of Geophysical Research: Atmospheres, 115, 10.1029/2010jd014007, 2010.

Ghatak, D., Deser, C., Frei, A., Gong, G., Phillips, A., Robinson, D. A., and Stroeve, J.: Simulated Siberian snow cover response to observed Arctic sea ice loss, 1979-2008, Journal of Geophysical Research: Atmospheres, 117, n/a-n/a, 10.1029/2012jd018047, 2012.

Gibson, C. E.: Silica Budgets and the Ecology of Planktonic Diatoms in an Unstratified Lake (Lough Neagh, N. Ireland), Internationale Revue der gesamten Hydrobiologie und Hydrographie, 66, 641-664, 10.1002/iroh.19810660502, 1981.

Gibson, C. E., Anderson, N. J., and Haworth, E. Y.: Aulacoseira subarctica: taxonomy, physiology, ecology and palaeoecology, European Journal of Phycology, 38, 83-101, 10.1080/0967026031000094102, 2003.

Gibson, C. E., Wang, G., and Foy, R. H.: Silica and diatom growth in Lough Neagh: the importance of internal recycling, Freshwater Biology, 45, 285-293, 10.1111/j.1365-2427.2000.00624.x, 2000.

Giglio, L., Boschetti, L., Roy, D. P., Humber, M. L., and Justice, C. O.: The Collection 6 MODIS burned area mapping algorithm and product, Remote Sens Environ, 217, 72-85, 10.1016/j.rse.2018.08.005, 2018.

Glückler, R., Herzschuh, U., Kruse, S., Andreev, A., Vyse, S. A., Winkler, B., Biskaborn, B. K., Pestryakova, L., and Dietze, E.: Wildfire history of the boreal forest of south-western Yakutia (Siberia) over the last two millennia documented by a lake-sediment charcoal record, Biogeosciences, 18, 4185-4209, 10.5194/bg-18-4185-2021, 2021.

Gorokhov, A. N. and Fedorov, A. N.: Current Trends in Climate Change in Yakutia, Geography and Natural Resources, 39, 153-161, 10.1134/s1875372818020087, 2018.

Hansen, M. C., Potapov, P. V., Moore, R., Hancher, M., Turubanova, S. A., Tyukavina, A., Thau, D., Stehman, S. V., Goetz, S. J., Loveland, T. R., Kommareddy, A., Egorov, A., Chini, L., Justice, C. O., and Townshend, J. R.: High-resolution global maps of 21st-century forest cover change, Science, 342, 850-853, 10.1126/science.1244693, 2013.

Hofmann, G., Lange-Bertalot, H., and Werum, M.: Diatomeen im Süßwasser-Benthos von Mitteleuropa: Bestimmungsflora Kieselalgen für die ökologische Praxis; über 700 der häufigsten Arten und ihre Ökologie, A.R.G. Gantner Verlag K.G., 9783906166926, 2011.

Hurrell, J. W.: Decadal trends in the north atlantic oscillation: regional temperatures and precipitation, Science, 269, 676-679, 10.1126/science.269.5224.676, 1995.

Hurrell, J. W. and Deser, C.: North Atlantic climate variability: The role of the North Atlantic Oscillation, Journal of Marine Systems, 79, 231-244, 10.1016/j.jmarsys.2009.11.002, 2010.

IAEA/WMO: Global Network for Isotopes in Precipitation. The GNIP Database. Accessible at: https://nucleus.iaea.org/wiser [dataset], 2023.

Jonsson, C. E., Rosqvist, G. C., Leng, M. J., Bigler, C., Bergman, J., Tillman, P. K., and Sloane, H. J.: High-resolution diatom δ18O records, from the last 150 years, reflecting changes in amount of winter precipitation in two sub-Arctic high-altitude lakes in the Swedish Scandes, Journal of Quaternary Science, 25, 918-930, https://doi.org/10.1002/jqs.1372, 2010.

Kandlbauer, J., Hopcroft, P. O., Valdes, P. J., and Sparks, R. S. J.: Climate and carbon cycle response to the 1815 Tambora volcanic eruption, Journal of Geophysical Research: Atmospheres, 118, 12,497-412,507, 10.1002/2013jd019767, 2013.

Kirillina, K., Shvetsov, E. G., Protopopova, V. V., Thiesmeyer, L., and Yan, W.: Consideration of anthropogenic factors in boreal forest fire regime changes during rapid socio-economic development: case study of forestry districts with increasing burnt area in the Sakha Republic, Russia, Environmental Research Letters, 15, 10.1088/1748-9326/ab6c6e, 2020.

Klein Tank, A. M. G., Wijngaard, J. B., Können, G. P., Böhm, R., Demarée, G., Gocheva, A., Mileta, M., Pashiardis, S., Hejkrlik, L., Kern-Hansen, C., Heino, R., Bessemoulin, P., Müller-Westermeier, G., Tzanakou, M., Szalai, S., Pálsdóttir, T., Fitzgerald, D., Rubin, S., Capaldo, M., Maugeri, M., Leitass, A., Bukantis, A., Aberfeld, R., van Engelen, A. F. V., Forland, E., Mietus, M., Coelho, F., Mares, C., Razuvaev, V., Nieplova, E., Cegnar, T., Antonio López, J., Dahlström, B., Moberg, A., Kirchhofer, W., Ceylan, A., Pachaliuk, O., Alexander, L. V., and Petrovic, P.: Daily dataset of 20th-century surface air temperature and precipitation series for the European Climate Assessment, International Journal of Climatology, 22, 1441-1453, 10.1002/joc.773, 2002.

https://doi.org/10.5194/cp-2023-85
Preprint. Discussion started: 7 November 2023

Kostrova, S. S., Meyer, H., Chapligin, B., Tarasov, P. E., and Bezrukova, E. V.: The last glacial maximum and late glacial environmental and climate dynamics in the Baikal region inferred from an oxygen isotope record of lacustrine diatom silica, Quatern Int, 348, 25-36, 10.1016/j.quaint.2014.07.034, 2014.

Kostrova, S. S., Meyer, H., Fernandoy, F., Werner, M., and Tarasov, P. E.: Moisture origin and stable isotope characteristics of precipitation in southeast Siberia, Hydrological Processes, 34, 51-67, 10.1002/hyp.13571, 2020.

Kostrova, S. S., Biskaborn, B. K., Pestryakova, L. A., Fernandoy, F., Lenz, M. M., and Meyer, H.: Climate and environmental changes of the Lateglacial transition and Holocene in northeastern Siberia: Evidence from diatom oxygen isotopes and assemblage composition at Lake Emanda, Quaternary Science Reviews, 259, 10.1016/j.quascirev.2021.106905, 2021.

Kostrova, S. S., Meyer, H., Chapligin, B., Bezrukova, E. V., Tarasov, P. E., and Kuz'min, M. I.: Reconstruction of the Holocene climate of Transbaikalia: Evidence from the oxygen isotope analysis of fossil diatoms from Kotokel Lake, Doklady Earth Sciences, 451, 732-736, 10.1134/S1028334x13070039, 2013a.

Kostrova, S. S., Meyer, H., Chapligin, B., Kossler, A., Bezrukova, E. V., and Tarasov, P. E.: Holocene oxygen isotope record of diatoms from Lake Kotokel (southern Siberia, Russia) and its palaeoclimatic implications, Quatern Int, 290, 21-34, 10.1016/j.quaint.2012.05.011, 2013b.

Kostrova, S. S., Meyer, H., Bailey, H. L., Ludikova, A. V., Gromig, R., Kuhn, G., Shibaev, Y. A., Kozachek, A. V., Ekaykin, A. A., and Chapligin, B.: Holocene hydrological variability of Lake Ladoga, northwest Russia, as inferred from diatom oxygen isotopes, Boreas, 48, 361-376, 10.1111/bor.12385, 2019.

Krammer, K. and Lange-Bertalot, H.: Bacillariophyceae, 4. Teil: Achnanthaceae, Kritische Ergänzungen zu Navicula (Lineolatae) und Gomphonema, Gesamtliteraturverzeichnis Teil 1 - 4, Süßwasserflora von Mitteleuropa, Band 2/4, Gustav Fischer Verlag, Stuttgart, Jena, 3437306642, 1991.

Krammer, K. and Lange-Bertalot, H.: Bacillariophyceae, 2. Teil: Bacillariaceae, Epithemiaceae, Surirellaceae, Süßwasserflora von Mitteleuropa, Band 2/2, Gustav Fischer Verlag, Jena, 3437353888, 1997a.

Krammer, K. and Lange-Bertalot, H.: Bacillariophyceae, 1. Teil: Naviculaceae, Süßwasserflora von Mitteleuropa, Band 2/1, Gustav Fischer Verlag, Jena, 3437353969, 1997b.

Krammer, K., Lange-Bertalot, H., Håkansson, H., and Nörpel, M.: Bacillariophyceae, 3. Teil: Centrales, Fragilariaceae, Eunotiaceae, Süßwasserflora von Mitteleuropa, Band 2/3, Gustav Fischer Verlag, Stuttgart, Jena, 3437305417, 1991.

Kruse, S., Bolshiyanov, D., Grigoriev, M. N., Morgenstern, A., Pestryakova, L., Tsibizov, L., and Udke, A.: Russian-German Cooperation: Expeditions to Siberia in 2018, https://doi.org/10.2312/BzPM_0734_2019, 2019.

Kurita, N., Yoshida, N., Inoue, G., and Chayanova, E. A.: Modern isotope climatology of Russia: A first assessment, Journal of Geophysical Research: Atmospheres, 109, n/a-n/a, 10.1029/2003jd003404, 2004.

Leclerc, A. J. and Labeyrie, L.: Temperature dependence of the oxygen isotopic fractionation between diatom silica and water, Earth and Planetary Science Letters, 84, 69-74, https://doi.org/10.1016/0012-821X(87)90177-4, 1987.

Leng, M. J. and Barker, P. A.: A review of the oxygen isotope composition of lacustrine diatom silica for palaeoclimate reconstruction, Earth-Science Reviews, 75, 5-27, 10.1016/j.earscirev.2005.10.001, 2006.

Leng, M. J. and Sloane, H. J.: Combined oxygen and silicon isotope analysis of biogenic silica, Journal of Quaternary Science, 23, 313-319, 10.1002/jqs.1177, 2008.

Leng, M. J., Swann, G. E. A., Hodson, M. J., Tyler, J. J., Patwardhan, S. V., and Sloane, H. J.: The Potential use of Silicon Isotope Composition of Biogenic Silica as a Proxy for Environmental Change, Silicon, 1, 65-77, 10.1007/s12633-009-9014-2, 2009.

Lenz, M. M., Andreev, A., Nazarova, L., Syrykh, L. S., Scheidt, S., Haflidason, H., Meyer, H., Brill, D., Wagner, B., Gromig, R., Lenz, M., Rolf, C., Kuhn, G., Fedorov, G., Svendsen, J. I., and Melles, M.: Climate, glacial and vegetation history of the polar Ural Mountains since c. 27 cal ka BP, inferred from a 54 m long sediment core from Lake Bolshoye Shchuchye, Journal of Quaternary Science, 37, 818-835, 10.1002/jqs.3400, 2021.

Liu, Y., An, W., Wang, X., and Xu, C.: Moisture history in the Northeast China since 1750s reconstructed from tree-ring cellulose oxygen isotope, Quatern Int, 10.1016/j.quaint.2022.03.009, 2022.

Mackay, A. W., Swann, G. E. A., Fagel, N., Fietz, S., Leng, M. J., Morley, D., Rioual, P., and Tarasov, P.: Hydrological instability during the Last Interglacial in central Asia: a new diatom oxygen isotope record from Lake Baikal, Quaternary Science Reviews, 66, 45-54, 10.1016/j.quascirev.2012.09.025, 2013.

https://doi.org/10.5194/cp-2023-85
Preprint. Discussion started: 7 November 2023

Manabe, S. and Stouffer, R. J.: Sensitivity of a global climate model to an increase of CO2concentration in the atmosphere, Journal of Geophysical Research, 85, 10.1029/JC085iC10p05529, 1980.

McKay, N. P. and Kaufman, D. S.: An extended Arctic proxy temperature database for the past 2,000 years, Sci Data, 1, 140026, 10.1038/sdata.2014.26, 2014.

Meister, P., Alexandre, A., Bailey, H., Barker, P., Biskaborn, B. K., Broadman, E., Cartier, R., Chapligin, B., Couapel, M., Dean, J. R., Diekmann, B., Harding, P., Henderson, A. C. G., Hernandez, A., Herzschuh, U., Kostrova, S. S., Lacey, J., Leng, M. J., Lücke, A., Mackay, A. W., Magyari, E. K., Narancic, B., Porchier, C., Rosqvist, G., Shemesh, A., Sonzogni, C., Swann, G. E. A., Sylvestre, F., and Meyer, H.: A global compilation of diatom silica oxygen isotope records from lake sediment – trends, and implications for climate reconstruction, in review 2023, Clim. Past Discuss. [preprint], 1-44, https://doi.org/10.5194/cp-2022-96, 2023.

Messager, M. L., Lehner, B., Grill, G., Nedeva, I., and Schmitt, O.: Estimating the volume and age of water stored in global lakes using a geo-statistical approach, Nat Commun, 7, 13603, 10.1038/ncomms13603, 2016.

Meyer, H., Chapligin, B., Hoff, U., Nazarova, L., and Diekmann, B.: Oxygen isotope composition of diatoms as Late Holocene climate proxy at Two-Yurts Lake, Central Kamchatka, Russia, Global and Planetary Change, 134, 118-128, 10.1016/j.gloplacha.2014.04.008, 2015.

Meyer, H., Schonicke, L., Wand, U., Hubberten, H. W., and Friedrichsen, H.: Isotope studies of hydrogen and oxygen in ground ice-experiences with the equilibration technique, Isotopes Environ Health Stud, 36, 133-149, 10.1080/10256010008032939, 2000.

Meyer, H., Kostrova, S. S., Meister, P., Lenz, M. M., Kuhn, G., Nazarova, L., Syrykh, L. S., and Dvornikov, Y.: Lacustrine diatom oxygen isotopes as palaeo precipitation proxy - Holocene environmental and snowmelt variations recorded at Lake Bolshoye Shchuchye, Polar Urals, Russia, Quaternary Science Reviews, 290, 10.1016/j.quascirev.2022.107620, 2022.

Miesner, T., Herzschuh, U., Pestryakova, L. A., Wieczorek, M., Zakharov, E. S., Kolmogorov, A. I., Davydova, P. V., and Kruse, S.: Forest structure and individual tree inventories of northeastern Siberia along climatic gradients, Earth Syst. Sci. Data, 14, 5695-5716, 10.5194/essd-14-5695-2022, 2022.

Miller, G. H., Alley, R. B., Brigham-Grette, J., Fitzpatrick, J. J., Polyak, L., Serreze, M. C., and White, J. W. C.: Arctic amplification: can the past constrain the future?, Quaternary Science Reviews, 29, 1779-1790, 10.1016/j.quascirev.2010.02.008, 2010.

Mock, C. J., Bartlein, P. J., and Anderson, P. M.: Atmospheric circulation patterns and spatial climatic variations in Beringia, International Journal of Climatology, 18, 1085-1104, 10.1002/(sici)1097-0088(199808)18:10<1085::Aid-joc305>3.0.Co;2-k, 1998.

Mollenhauer, G., Grotheer, H., Gentz, T., Bonk, E., and Hefter, J.: Standard operation procedures and performance of the MICADAS radiocarbon laboratory at Alfred Wegener Institute (AWI), Germany, Nuclear Instruments and Methods in Physics Research Section B: Beam Interactions with Materials and Atoms, 496, 45-51, 10.1016/j.nimb.2021.03.016, 2021.

Morley, D. W., Leng, M. J., Mackay, A. W., Sloane, H. J., Rioual, P., and Battarbee, R. W.: Cleaning of lake sediment samples for diatom oxygen isotope analysis, Journal of Paleolimnology, 31, 391-401, 10.1023/B:JOPL.0000021854.70714.6b, 2004.

Moschen, R., Lücke, A., and Schleser, G. H.: Sensitivity of biogenic silica oxygen isotopes to changes in surface water temperature and palaeoclimatology, Geophysical Research Letters, 32, n/a-n/a, 10.1029/2004gl022167, 2005.

Osborn, T. J.: Recent variations in the winter North Atlantic Oscillation, Weather, 61, 353-355, 10.1256/wea.190.06, 2006.

Overland, J. E. and Wang, M.: The 2020 Siberian heat wave, International Journal of Climatology, 41, 10.1002/joc.6850, 2020.

Philippsen, B.: The freshwater reservoir effect in radiocarbon dating, Heritage Science, 1, 10.1186/2050-7445-1-24, 2013.

Previdi, M., Smith, K. L., and Polvani, L. M.: Arctic amplification of climate change: a review of underlying mechanisms, Environmental Research Letters, 16, 10.1088/1748-9326/ac1c29, 2021.

Rantanen, M., Karpechko, A. Y., Lipponen, A., Nordling, K., Hyvärinen, O., Ruosteenoja, K., Vihma, T., and Laaksonen, A.: The Arctic has warmed nearly four times faster than the globe since 1979, Communications Earth & Environment, 3, 10.1038/s43247-022-00498-3, 2022.

https://doi.org/10.5194/cp-2023-85
Preprint. Discussion started: 7 November 2023

Reimer, P. J., Austin, W. E. N., Bard, E., Bayliss, A., Blackwell, P. G., Bronk Ramsey, C., Butzin, M., Cheng, H., Edwards, R. L., Friedrich, M., Grootes, P. M., Guilderson, T. P., Hajdas, I., Heaton, T. J., Hogg, A. G., Hughen, K. A., Kromer, B., Manning, S. W., Muscheler, R., Palmer, J. G., Pearson, C., van der Plicht, J., Reimer, R. W., Richards, D. A., Scott, E. M., Southon, J. R., Turney, C. S. M., Wacker, L., Adolphi, F., Büntgen, U., Capano, M., Fahrni, S. M., Fogtmann-Schulz, A., Friedrich, R., Köhler, P., Kudsk, S., Miyake, F., Olsen, J., Reinig, F., Sakamoto, M., Sookdeo, A., and Talamo, S.: The IntCal20 Northern Hemisphere Radiocarbon Age Calibration Curve (0–55 cal kBP), Radiocarbon, 62, 725-757, 10.1017/rdc.2020.41, 2020.

Rosqvist, G. C., Rietti-Shati, M., and Shemesh, A.: Late glacial to middle Holocene climatic record of lacustrine biogenic silica oxygen isotopes from a Southern Ocean island, Geology, 27, 967-970, Doi 10.1130/0091-7613(1999)027<0967:Lgtmhc>2.3.Co;2, 1999.

Rosqvist, G. C., Leng, M. J., Goslar, T., Sloane, H. J., Bigler, C., Cunningham, L., Dadal, A., Bergman, J., Berntsson, A., Jonsson, C., and Wastegård, S.: Shifts in precipitation during the last millennium in northern Scandinavia from lacustrine isotope records, Quaternary Science Reviews, 66, 22-34, 10.1016/j.quascirev.2012.10.030, 2013.

Rutkowski, C., Lenz, J., Lang, A., Wolter, J., Mothes, S., Reemtsma, T., Grosse, G., Ulrich, M., Fuchs, M., Schirrmeister, L., Fedorov, A., Grigoriev, M., Lantuit, H., and Strauss, J.: Mercury in sediment core samples from deep Siberian ice-rich permafrost, Frontiers in Earth Science, 9, 10.3389/feart.2021.718153, 2021.

Sato, T., Nakamura, T., Iijima, Y., and Hiyama, T.: Enhanced Arctic moisture transport toward Siberia in autumn revealed by tagged moisture transport model experiment, npj Climate and Atmospheric Science, 5, 10.1038/s41612-022-00310-1, 2022.

Scholten, R. C., Coumou, D., Luo, F., and Veraverbeke, S.: Early snowmelt and polar jet dynamics co-influence recent extreme Siberian fire seasons, Science, 378, 1005-1009, 10.1126/science.abn4419, 2022.

Seneviratne, S. I., X. Zhang, M. Adnan, W. Badi, C. Dereczynski, A. Di Luca, S. Ghosh, I. Iskandar, J. Kossin, S. Lewis, F. Otto, I. Pinto, M. Satoh, S.M. Vicente-Serrano, M. Wehner, and Zho, B.: Weather and Climate Extreme Events in a Changing Climate, in: Climate Change 2021: The Physical Science Basis. Contribution of Working Group I to the Sixth Assessment Report of the Intergovernmental Panel on Climate Change [Masson-Delmotte, V., P. Zhai, A. Pirani, S.L. Connors, C. Péan, S. Berger, N. Caud, Y. Chen, L. Goldfarb, M.I. Gomis, M. Huang, K. Leitzell, E. Lonnoy, J.B.R. Matthews, T.K. Maycock, T. Waterfield, O. Yelekçi, R. Yu, and B. Zhou (eds.)], Cambridge University Press, Cambridge, United Kingdom and New York, NY, USA, 1513–1766, 10.1017/9781009157896.013, 2021.

Shahgedanova, M.: Climate at present and in the historical past, The physical geography of northern Eurasia, 70-102, 2002.

Shemesh, A. and Peteet, D.: Oxygen isotopes in fresh water biogenic opal - Northeastern US Alleröd-Younger Dryas temperature shift, Geophysical Research Letters, 25, 1935-1938, 10.1029/98gl01443, 1998.

Shemesh, A., Rosqvist, G., Rietti-Shati, M., Rubensdotter, L., Bigler, C., Yam, R., and Karlén, W.: Holocene climatic change in Swedish Lapland inferred from an oxygen-isotope record of lacustrine biogenic silica, The Holocene, 11, 447-454, 10.1191/095968301678302887, 2001.

Stenchikov, G., Delworth, T. L., Ramaswamy, V., Stouffer, R. J., Wittenberg, A., and Zeng, F.: Volcanic signals in oceans, Journal of Geophysical Research, 114, 10.1029/2008jd011673, 2009.

Stuiver, M. and Reimer, P. J.: A Computer Program for Radiocarbon Age Calibration, Radiocarbon, 28, 1022-1030, 10.1017/S0033822200060276, 1986.

Stuiver, M. and Reimer, P. J.: Extended 14C Data Base and Revised CALIB 3.0 14C Age Calibration Program, Radiocarbon, 35, 215-230, 10.1017/S0033822200013904, 1993.

Sun, C., Li, J., and Zhao, S.: Remote influence of Atlantic multidecadal variability on Siberian warm season precipitation, Sci Rep, 5, 16853, 10.1038/srep16853, 2015.

Swann, G. E. A. and Leng, M. J.: A review of diatom δ18O in palaeoceanography, Quaternary Science Reviews, 28, 384-398, 10.1016/j.quascirev.2008.11.002, 2009.

Swann, G. E. A., Leng, M. J., Juschus, O., Melles, M., Brigham-Grette, J., and Sloane, H. J.: A combined oxygen and silicon diatom isotope record of Late Quaternary change in Lake El'gygytgyn, North East Siberia, Quaternary Science Reviews, 29, 774-786, 10.1016/j.quascirev.2009.11.024, 2010.

Swann, G. E. A., Mackay, A. W., Vologina, E., Jones, M. D., Panizzo, V. N., Leng, M. J., Sloane, H. J., Snelling, A. M., and Sturm, M.: Lake Baikal isotope records of Holocene Central Asian precipitation, Quaternary Science Reviews, 189, 210-222, 10.1016/j.quascirev.2018.04.013, 2018.

https://doi.org/10.5194/cp-2023-85
Preprint. Discussion started: 7 November 2023

Tomshin, O. and Solovyev, V.: Features of the Extreme Fire Season of 2021 in Yakutia (Eastern Siberia) and Heavy Air Pollution Caused by Biomass Burning, Remote Sensing, 14, 10.3390/rs14194980, 2022.

Trouet, V., Esper, J., Graham, N. E., Baker, A., Scourse, J. D., and Frank, D. C.: Persistent positive North Atlantic oscillation mode dominated the Medieval Climate Anomaly, Science, 324, 78-80, 10.1126/science.1166349, 2009.

van Hardenbroek, M., Chakraborty, A., Davies, K. L., Harding, P., Heiri, O., Henderson, A. C. G., Holmes, J. A., Lasher, G. E., Leng, M. J., Panizzo, V. N., Roberts, L., Schilder, J., Trueman, C. N., and Wooller, M. J.: The stable isotope composition of organic and inorganic fossils in lake sediment records: Current understanding, challenges, and future directions, Quaternary Science Reviews, 196, 154-176, 10.1016/j.quascirev.2018.08.003, 2018.

Vyse, S. A., Herzschuh, U., Andreev, A. A., Pestryakova, L. A., Diekmann, B., Armitage, S. J., and Biskaborn, B. K.: Geochemical and sedimentological responses of arctic glacial Lake Ilirney, chukotka (far east Russia) to palaeoenvironmental change since ~51.8 ka BP, Quaternary Science Reviews, 247, 10.1016/j.quascirev.2020.106607, 2020.

Wang, L., Mackay, A. W., Leng, M. J., Rioual, P., Panizzo, V. N., Lu, H., Gu, Z., Chu, G., Han, J., and Kendrick, C. P.: Influence of the ratio of planktonic to benthic diatoms on lacustrine organic matter δ13C from Erlongwan maar lake, northeast China, Organic Geochemistry, 54, 62-68, 10.1016/j.orggeochem.2012.09.010, 2013.

Wang, Q., Kim, D., Dionysiou, D. D., Sorial, G. A., and Timberlake, D.: Sources and remediation for mercury contamination in aquatic systems--a literature review, Environ Pollut, 131, 323-336, 10.1016/j.envpol.2004.01.010, 2004.

Wegmann, M., Orsolini, Y., Vázquez, M., Gimeno, L., Nieto, R., Bulygina, O., Jaiser, R., Handorf, D., Rinke, A., Dethloff, K., Sterin, A., and Brönnimann, S.: Arctic moisture source for Eurasian snow cover variations in autumn, Environmental Research Letters, 10, 10.1088/1748-9326/10/5/054015, 2015.

Wetterich, S., Herzschuh, U., Meyer, H., Pestryakova, L., Plessen, B., Lopez, C. M. L., and Schirrmeister, L.: Evaporation effects as reflected in freshwaters and ostracod calcite from modern environments in Central and Northeast Yakutia (East Siberia, Russia), Hydrobiologia, 614, 171-195, 10.1007/s10750-008-9505-y, 2008.

Wolin, J. A. and Stone, J. R.: Diatoms as Indicators of Water-level Change in Freshwater Lakes, The Diatoms Applications to the Environmental and Earth Sciences, 174-185, 2010.

Ye, H. C., Cho, H. R., and Gustafson, P. E.: The changes in Russian winter snow accumulation during 1936-83 and its spatial patterns, Journal of Climate, 11, 856-863, 10.1175/1520-0442(1998)011<0856:Tcirws>2.0.Co;2, 1998.

Zielinski, G. A., Mayewski, P. A., Meeker, L. D., Whitlow, S., Twickler, M. S., Morrison, M., Meese, D. A., Gow, A. J., and Alley, R. B.: Record of Volcanism Since 7000 B.C. from the GISP2 Greenland Ice Core and Implications for the Volcano-Climate System, Science, 264, 948-952, 10.1126/science.264.5161.948, 1994.